Aalto University
School of Science

Olli Heikkinen

X-Ray Photoelectron Spectroscopic Studies of Laboratory-Aged Natural Gas and Diesel Oxidation Catalysts

Licentiate thesis submitted in partial fulfillment of the requirements for the degree of Licentiate of Science in Technology in Aalto Doctoral Programme in Science.

Espoo, 28.8.2015

Aalto University School of Science
Department of Applied Physics
Surface Science Group

Supervisor: Prof. Peter Liljeroth
Instructor: Dr. Jouko Lahtinen

Aalto University
School of Science

Abstract of Licentiate Thesis

Author

Heikkinen, Olli Veikko

Title of Thesis

X-Ray Photoelectron Spectroscopic Studies of Laboratory-Aged Natural Gas and Diesel Oxidation Catalysts

Abstract

Combustion engines are a major source of emissions such as various greenhouse gases and hazardous chemicals. Reducing these emissions is of major importance, and catalytic converters are one of the most prominent applications towards this end. In a catalytic converter, molecules in the exhaust gas undergo oxidation or reduction reactions enhanced by noble metal catalysts and form less harmful compounds.

While in use, the catalytic converters and the active catalytic materials within are gradually deactivated. In chemical poisoning, unwanted particles adsorb on the active sites of the catalyst thus preventing adsorption and conversion of the desired molecules. In thermal deactivation, the active catalyst particles migrate to form larger particles, thus decreasing the active surface area of the catalyst.

In this work, the effect of laboratory-scale deactivation treatments on diesel and natural gas oxidation catalysts are studied. All the catalysts feature platinum or palladium as the active metal and alumina, silica or zirconia as the solid support. In the deactivation treatments, the catalysts have been exposed to sulfur and phosphorus, significant catalytic poisons, as well as elevated temperatures.

The effect of these treatments have been investigated with X-ray photoelectron spectroscopy, a non-destructive experimental method for chemical characterization. The atomic percentages of the chemical elements in each catalyst have been determined together with the chemical states of each element. With the help of complementary studies, the properties of the treated catalysts are discussed in detail.

Research field	Key words
Engineering Physics, Physics	**catalysis, deactivation, diesel, natural gas, phosphorus, sulfur, XPS**
Supervising professor	**Pages**
Prof. Peter Liljeroth	**58**
Thesis advisor	**Language**
Dr. Jouko Lahtinen	**English**
Thesis examiner	**Date**
Dr. Joseph Campbell	**28.8.2015**

☒ **The thesis can be read at https://aaltodoc.aalto.fi/handle/123456789/27**

Aalto-yliopisto
Perustieteiden korkeakoulu

Lisensiaatintutkimuksen tiivistelmä

Tekijä

Heikkinen, Olli Veikko

Lisensiaatintutkimuksen nimi

Laboratorioikäytettyjen maakaasu- ja dieselhapetuskatalyyttien tutkimuksia röntgenfotoelektronispektroskopialla

Tiivistelmä

Polttomoottorit ovat erilaisten päästöjen, kuten kasvihuonekaasujen ja terveydelle haitallisten kemikaalien merkittävä lähde. Päästöjen vähentäminen on tärkeää, ja eräs merkittävimmistä sovelluksista tämän saavuttamiseksi ovat katalysaattorit. Katalysaattorissa pakokaasun molekyylit hapettuvat tai pelkistyvät jalometallisten katalyyttien mahdollistamissa reaktioissa muodostaakseen vähemmän haitallisia yhdisteitä.

Käytössä katalysaattorit, ja niiden katalyyttisesti aktiivinen materiaali, deaktivoituvat vähitellen. Myrkyttyminen tarkoittaa tilannetta, jossa ei-toivotut yhdisteet adsorboituvat katalyytin pinnalle ja näin estävät haluttujen molekyylien adsorption ja niiden katalyyttiset reaktiot. Termisessä deaktivaatiossa aktiiviset katalyyttihiukkaset yhdistyvät suuremmiksi hiukkasiksi, jolloin katalyyttisesti aktiivinen pinta-ala pienenee.

Tässä työssä tutkitaan laboratorio-olosuhteissa tehtyjen ikäytyskokeiden vaikutuksia diesel- ja maakaasumoottorien hapetuskatalyytteihin. Tutkimuksen kaikissa katalyyteissä aktiivinen aine on platinaa tai palladiumia, ja kantaja-aineena on alumiini-, pii- tai zirkoniumoksidi. Ikäytyskokeissa katalyytit on altistettu rikille ja fosforille, jotka ovat merkittäviä katalyyttimyrkkyjä, sekä korkeille lämpötiloille.

Ikäytysten vaikutusta on tutkittu kokeellisesti röntgenfotoelektronispektroskopialla. Kunkin katalyytin alkuaineiden atomiprosenttiosuudet sekä kunkin alkuaineen kemiallinen tila on määritetty. Viittaamalla lisäksi muilla menetelmillä saatuihin täydentäviin tuloksiin työssä esitellään yksityiskohtaisesti ikäytettyjen katalyyttien ominaisuuksia.

Tutkimusala **Teknillinen fysiikka, fysiikka**	**Avainsanat** **deaktivaatio, diesel, fosfori, katalyysi, maakaasu, rikki, XPS**
Vastuuprofessori **Prof. Peter Liljeroth**	**Sivumäärä** **58**
Ohjaaja **TkT Jouko Lahtinen**	**Kieli** **englanti**
Työn tarkastaja **Dr. Joseph Campbell**	**Päiväys** **28.8.2015**

☒ **Luettavissa verkossa osoitteessa https://aaltodoc.aalto.fi/handle/123456789/27**

Preface

This work is a report of experimental catalyst studies carried out in Aalto University in 2013 and 2014 as a part of the Academy of Finland project ACaBio. These measurements have been sort of a sidetrack in my doctoral studies and thus they deserved a thesis in their own right. Besides, I have even learned a lot about emission reduction technology while writing it.

I would like to thank my instructor, our group leader Dr. Jouko Lahtinen for giving me the responsibility for this project and helping me try and understand our results whenever needed. I am also much obliged to Prof. Peter Liljeroth for acting as the supervisor. In addition, many thanks go to Minna Kauppila and Maaria Salmi for carrying out many of the actual experiments, and to the ACaBio people in Oulu and Tampere for the pleasant and fruitful collaboration. And finally, I am of course very grateful for my friends and family for being there

Now, back to the doctoral studies.

Otaniemi, 28.8.2015

Olli Heikkinen

Contents

1 Introduction

For the last hundred years, combustion engines have been a significant source for unwanted emissions. These emissions include carbon monoxide, carbon dioxide, oxides of nitrogen and organic hydrocarbon molecules. Some of these gases are hazardous to health and all are greenhouse gases that contribute to the greenhouse effect and global warming. It is of major importance to decrease the release of these pollutants. Within the last few decades, work towards this end has been done by the means of the technological development of fuels and engines. Simultaneously, stricter legislative measures have been set to reduce the emission caused by vehicles. As an example of this, the Euro 6 emission norm was put into action as recently as in September 2014 [1].

One of the greatest milestones in emission control has been the introduction of catalytic converters in the 1970s. The catalytic converter is a part of the postcombustion line where exhaust gas molecules undergo oxidation and reduction reactions enhanced by noble metal catalysts. The reactions transform the emission molecules into less hazardous compounds. Nowadays catalytic converters are a standard component in vehicles but improving their efficiency and compatibility with new fuels keeps their development a relevant task.

Catalyst materials in the catalytic converter can undergo gradual deactivation, i.e. the decrease of the conversion rate, for various reasons. Thermal conditions in the exhaust line may cause structural changes in the catalyst, and some particles may adsorb irreversibly on the catalytic surface preventing further reactions, thus chemically poisoning the catalyst. Deactivation mechanisms and consequences need to be studied in order to develop more durable catalytic converters.

In this work, deactivation of platinum and palladium catalysts for diesel and natural gas oxidation was studied. The catalysts had undergone laboratory-scale treatments resulting in chemical poisoning by phosphorus and sulfur as well as thermal deactivation. This work reports chemical properties of the catalysts and their changes as observed by X-ray photoelectron spectroscopy (XPS), an experimental method for chemical characterization. These studies were a part of Academy of Finland project ACaBio (Advanced Catalytic Materials for Biofuels' Emission Reduction). The purpose of this thesis is to serve as documentation of all XPS studies carried out within this project in 2013 and 2014.

2 Automotive exhaust gas catalysis

2.1 Vehicle emissions

Vehicles powered by combustion engines are a remarkable source of pollutants in the atmosphere. Complete or partial burning of fuels produces exhaust gases which are emitted into the air. In exhaust gases there are many chemicals that are medically hazardous or harmful to the environment. The exact composition of the emission depends on the fuel and engine types, but the fundamental problem is universal.

In principle, full combustion of fuel produces only water (H_2O) and carbon dioxide (CO_2) [2]. The latter is not toxic or hazardous to health but it is a significant greenhouse gas and thus strongly contributes to global warming [3]. Improved technology, such as more economic engines and fuels with higher hydrogen-to-carbon ratios, has diminished CO_2 emissions throughout the last decades. However, there is currently no technology to gain zero CO_2 emission [4].

The major pollutants in exhaust gases are carbon monoxide (CO), various hydrocarbons (HC) and nitrogen oxides (NO_x). HC and CO are formed due to incomplete combustion. Hydrocarbon molecules may also remain intact through the engine and contribute to the emission. Production of NO_x occurs at temperatures higher than 1500 degrees centigrade when nitrogen originating from the air reacts with oxygen inside the engine. Carbon monoxide is toxic and lethal in high concentrations. Hydrocarbons in the atmosphere may also contribute to several medical conditions. Furthermore, HC and NO_x are major contributors for ground-level ozone and smog. [2]

In addition, exhaust gas may contain sulfur dioxide (SO_2) and soluble or volatile organic fraction (SOF, VOF), which means larger, carcinogenic organic molecules. Beside these gaseous components, the vehicle emissions also includes solid particulate matter, such as soot. Particulate matter has been found to be correlated to some respiratory illnesses. [2, 5, 6]

On-going technological development has decreased automobile emissions during the last decades. Petroleum industry has developed new fuels whereas automotive industry has provided more efficient engines and after-treatment methods like catalytic converters. Moreover, legislative acts for emission limits have been set into effect worldwide (eg. Euro 5 and Euro 6 regulations [1]).

2.2 Catalytic converters

In chemistry, catalysis means a reaction where an additional substance, called catalyst, offers an alternative reaction pathway that decreases the activation energy of the rate-limiting step, thus increasing the rate of the reaction. The catalyst itself is not consumed in the reaction.

Catalysis is used for advantage in vehicle emission reduction processes. A catalytic converter is a part of the postcombustion exhaust line. Its purpose is to be a site for reactions that transform molecules in exhaust gas into a less harmful form. Hydrocarbons and carbon monoxide are oxidized, carbon dioxide being the desired product of the reactions. Basic oxidation reactions are [2]

$$\mathrm{C}_m\mathrm{H}_n + (1 + \frac{n}{4})\mathrm{O}_2 \rightarrow m\mathrm{CO}_2 + \frac{n}{2}\mathrm{H}_2\mathrm{O}, \tag{1}$$

$$\mathrm{CO} + \frac{1}{2}\mathrm{O}_2 \rightarrow \mathrm{CO}_2, \tag{2}$$

$$\mathrm{CO} + \mathrm{H}_2\mathrm{O} \rightarrow \mathrm{CO}_2 + \mathrm{H}_2. \tag{3}$$

Hence, catalytic converters aim at producing carbon dioxide, which is a greenhouse gas itself, albeit much less harmful than the initial HC and CO molecules. Nitrogen oxides are converted into molecular nitrogen, harmless and the most abundant particle in the atmosphere. The basic reduction reactions are [2]

$$\mathrm{NO} + \mathrm{CO} \rightarrow \frac{1}{2}\mathrm{N}_2 + \mathrm{CO}_2, \tag{4}$$

$$\mathrm{NO} + \mathrm{H}_2 \rightarrow \frac{1}{2}\mathrm{N}_2 + \mathrm{H}_2\mathrm{O}. \tag{5}$$

The reactions 4 and 5 are valid for NO_2 as well with different stoichiometric ratios. A catalyst where all three types of conversion reactions take place is called a three-way catalyst (TWC). Depending on the application, there are also catalytic converters that are able to enhance only either oxidation or reduction. For all three reactions, a conversion rate of 90% is commercially achievable, although not for all types of engines or operating conditions [2]. It has been estimated that already before the year 2000 catalytic converters had reduced the total emissions of CO, HC and NO_x by 800 million tons [7].

A typical catalytic converter structure is illustrated in figure 1. In addition, figure 2 shows the structure of the converters studied in this work. The converter is a metallic or ceramic tube through which the exhaust gas flows. It has an internal, again metallic or ceramic, honeycomb-like or monolithic structure dividing the tube into numerous smaller channels. The walls of

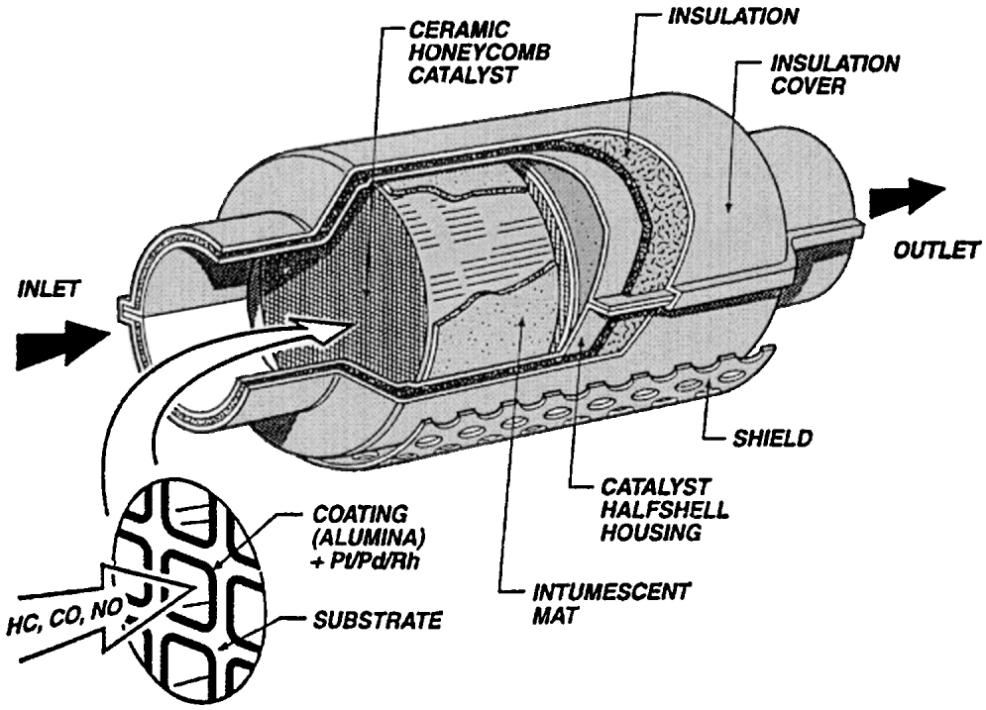

Figure 1: A schematic illustration of a catalytic converter. Copyright 2001 Elsevier. Reproduced with permission from Reference [2].

these inner structure are coated by a metal oxide washcoat, and the actual catalyst particles are dispersed throughout the washcoat. The catalyst particles are some noble metal or metal oxide clusters. Initially, platinum and rhodium were the main catalytic metals in exhaust gas conversion, but since the introduction of lead-free fuels palladium has also become a prominent alternative [10]. The catalytic reactions take place on the washcoat surface, and hence as large as possible surface area to bulk volume ratio is a desirable property of the washcoat. Therefore, porous materials are widely used, aluminum oxide (alumina, Al_2O_3) being a very typical choice. In addition, the washcoat often includes other metal oxides for enhancing the operation. For instance, ceria (CeO_2) is used as a oxygen storage components, aiding oxidation reactions in fuel-rich operating conditions [11]. Zirconia (ZrO_2) on the other hand increases thermal stability and platinum dispersion [12].

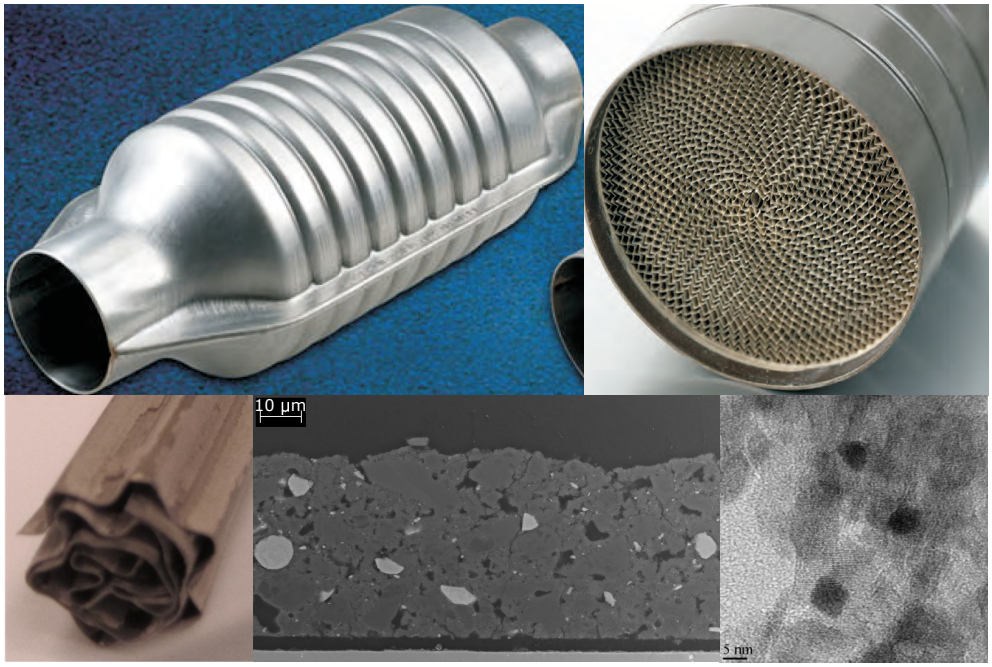

Figure 2: The basic structure of catalyst samples studied in this work. The catalytic converter is a steel shielded honeycomb. The honeycomb surface has been coated with a porous washcoat and the catalyst itself is dispersed in the washcoat. Modified after [8, 9].

2.3 Diesel oxidation catalysis

Some of the catalysts studied in this work have been designed for oxidation reactions in diesel engines. Diesel engines operate in lean conditions, which means there is a significant excess of air against fuel. Among the emissions, there is CO, HC and NO_x, SOF originating from lubricating oils, sulfur oxides and soot. [2]

A diesel oxidation catalyst (DOC) oxidizes CO and HC according to equations 1-2. A simultaneous oxidation of SO_2 to SO_3 is not desirable, since that would further lead to increase in sulfuric acid production. Three-way catalysis is not possible in diesel engines, since due to the lean conditions nitrogen oxide reduction cannot be achieved. Instead, oxidation of nitrogen monoxide

$$\mathrm{NO} + \frac{1}{2}\mathrm{O_2} \rightarrow \mathrm{NO_2} \tag{6}$$

is significant at moderate temperatures [13]. This is actually a wanted reaction, since NO_2 accelerates soot oxidation process [14]. Furthermore, NO_x

reduction is carried out in a separate catalyst after DOC with a use of selective catalytic reduction (SCR) or NO_x storage and reduction (NSR) catalysts. It has been found that reduction rates are increased if the NO is first oxidized into dioxidic form [15]. In addition, diesel engines apply a particulate filter to reduce the emission of soot and other solid matter. Thus, DOC by itself is not enough for emission control in diesel-powered vehicles.

2.4 Natural gas oxidation catalysis

A part of the samples studied in this work were natural gas oxidation (NGO) catalysts. NGO catalysis as well as natural gas engines are a relatively new technology and still have only a minor role in the market. A lean burn natural gas engine has been reported to produce less particulate matter and nitrogen oxide emissions than a diesel engine of comparable power [16].

Methane (CH_4) is the major component of natural gas, and a significant fraction of methane molecules survives through the combustion engine, contributing to the emissions of natural gas. Methane is a greenhouse gas, predicted to be more than an order of magnitude more active than CO_2 [17]. Thus NGO catalysts have to be able to efficiently oxidize methane. The oxidation reaction is a special case of equation 1,

$$CH_4 + 2O_2 \rightarrow CO_2 + 2H_2O. \tag{7}$$

However, the stability of methane and relatively low operating temperatures in a natural gas engine make the conversion more challenging. In lean conditions PdO has been found to be the most efficient catalyst [18]. Similarly to DOCs, an NGO catalyst must also be able to oxidize CO.

2.5 Catalyst deactivation

Catalyst deactivation is a process where the active particles are in some way prevented from taking part in the reactions taking place on the catalyst surface. Deactivation can be complete or partial, and often it is also gradual, increasing as a function of time. Furthermore, the reasons behind deactivation may be chemical or physical, and the process may be reversible or irreversible.

Catalytic converters for combustion engines undergo deactivation due to the chemical and thermodynamical conditions in the converter. The deactivation processes are often complex, but in a simplified fashion, deactivation can be divided into four main classes; poisoning, sintering, phase transformation and

coking [19]. The schematic drawings in figure 3 illustrate these phenomena.

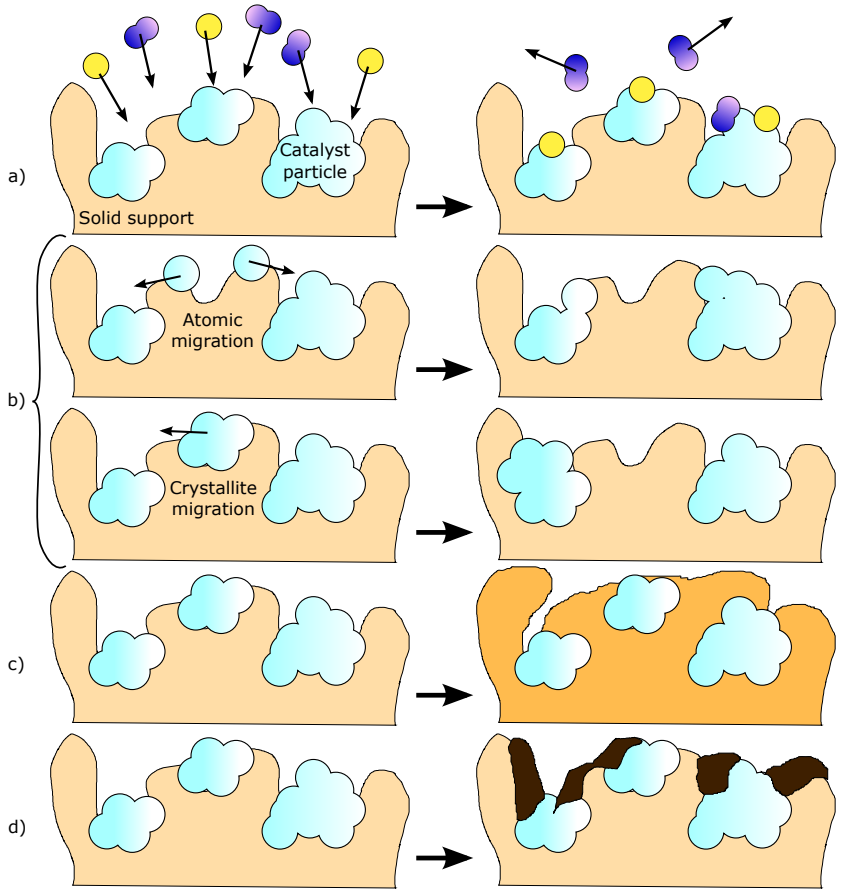

Figure 3: The main mechanisms for catalyst deactivation. (a) Chemical poisoning, i.e. chemisorption of impurity particles on active sites. (b) Sintering causes particle size growth thus altering the catalytic properties. (c) Solid-state phase transformation of the support blocks the catalyst particles. (d) Coking, i.e. blockage of catalyst particles by residual carbon compounds. The sizes in the image are not to scale.

Poisoning means chemisorption of particles that alter the behaviour of the catalyst. The poison particles may have a geometric blocking effect by adsorbing on the active sites, leaving less or no sites for the molecules to be converted to be adsorbed on. They can also reduce the adsorptivity of the catalyst through an electronic effect. Furthermore, they can also form molecules with the active particles and thus strongly alter the surface chemistry of the catalyst. [19]

The poisoning effect can be selective or non-selective. In non-selective poisoning every adsorption site is equally probable to get an impurity particle, and in selective poisoning there is a bias towards more active sites. There is also anti-selective poisoning where the poison particles prefer sites of lesser activity. [20] In reversible poisoning the particles are only weakly adsorbed. Desorption can happen relatively easily, and removing the particle from the feedstock may completely undo the deactivation. Instead of poisoning, these processes are often called inhibition. If poisoning is irreversible, stronger adsorption or further changes take place, making the deactivation permanent. [21]

In oxidation catalysis there are many elements that can act as catalytic poisons. Historically, the most prominent is probably lead which forms compounds directly with palladium, and reacts with other impurities on platinum catalyst surfaces [10]. Due to this strong deactivation effect, catalytic converters became an integral part of exhaust lines only after the introduction of lead-free fuel. Nowadays there are still many poisoning chemicals as minor components in fuels, lubricant oils or oil additives, for example zinc, calcium, sulfur and phosphorus [21]. The latter two are poisons which are also studied in this work. Of these two, sulfur has been studied more widely in literature.

Many fuels include small fractions of sulfur. It is present in organic compounds of many forms. It is generally oxidized to SO_2 during the combustion, and an oxidizing catalyst can further oxidize it to SO_3. Typically, 5% of SO_2 is adsorbed on the catalyst surface. SO_3 is strongly acidic, and can react with catalyst components thus forming sulfates (SO_4^{2-}). However, if SO_2 does not undergo further reactions, the deactivation mechanism is generally stronger than that of sulfates. Sulfur has been found to be distributed quite homogeneously from inlet to outlet, and from surface to bottom. Dihydrogen sulfide (H_2S) is even stronger poison for metals, and it forms in oxygen deficient conditions. [21]

The effect of sulfur depends on the catalyst and support materials. Sulfur trioxide reacts with palladium forming palladium sulfate. Oxidation reactions on palladium catalyst surfaces are highly deactivated by sulfur. For instance, methane oxidation is totally inhibited with a 1 ppm fraction of SO_2. Platinum, on the other hand, is more resistant towards sulfur poisoning. [17] For instance, platinum is an efficient catalyst for oxidizing SO_2 into SO_3. However, it does not adsorb SO_3 at all which diminishes deactivation. In fact, through somewhat complex effects, HC oxidation activity has been

reported to even increase due to SO_2 adsorption. In NO reduction catalysis, SO_2 has been reported to have a greater deactivation effect on platinum than on palladium. Alumina and ceria are supports that react and form sulfates with sulfur. This can alter the interaction between the noble metal and the sulfur and therefore weaken the catalytic properties. Silica and zirconia are non-sulfating supports and do not adsorb sulfur. As a consequence, deactivation can be more efficient since reactions with sulfur and the catalytic metal become more selective. On the other hand, the reversibility may improve, if sulfur needs to be desorbed from the catalytic metal sites only. [21]

Phosphorus compounds in the exhaust line originate from lubricating oils and additives. In particular, phosphorus can be found in zinc dialkyldithiophosphate, an antiwear and antioxidant additive [22]. Phosphorus compounds are in general strong catalytic poisons, possibly more severe than lead, providing irreversible deactivation.

In a combustion engine feedstock, phosphorus often appears in phosphate (PO_4^{3-}) compounds, and it has been reported to further form new phosphate compounds during the process [21]. It can react with zinc, calcium and magnesium found in other additives and form an overlayer on the catalyst surface. Alternatively, it can react directly with washcoat particles, such as alumina or ceria and form phosphates with them. [22] It has also been reported that phosphorus adsorption rate is not influenced by the type of the washcoat or the presence of catalytic metal (Pt) [23]. Phosphorus adsorption is selective, as it prefers sites on the surface in the inlet section of the catalyst [21].

Phosphorus poisoning has been diminished with adsorption of calcium and barium [21]. They are catalyst poisons themselves and compete for same adsorption sites. Some regeneration has been gained with oxalic acid treatment [22]. However, decreasing phosphoric components in oil additives has appeared to be the most efficient way to avoid phosphorus poisoning.

Sintering is physical deactivation caused by thermodynamic effects. It means particle size growth through migration processes. Two models have been suggested, atomic and crystallite migration. In the former, atoms escape from crystallites, travel on the catalyst surface and collide with larger crystallites, binding with them. In the latter, whole crystallites diffuse along the catalyst surface, collide and unite. Either case gives rise to crystallites of larger size. Sintering is mainly temperature dependent, as it takes place when heat overcomes the activation energy of migration, and its degree of occurrence is increased as a function of temperature. Furthermore, sudden changes of

temperature may also cause sintering. [21]

Larger particles decrease the surface area and thus the number of catalytically active sites, causing deactivation. Along with sintering, temperature changes may change also electric and chemical properties of the active particles. For example platinum oxide is reduced to metallic platinum above 600 °C, which is a relevant temperature in three-way catalysis. Washcoat materials may also undergo sintering. This may result in disappearance of pores on the surface and encapsulation of active particles. Solid-state phase transformations are an extreme form of sintering. There, structural changes take place not only through particle size changes but also through the complete change of crystallite phase. Some sintering effects can be decreased and some of the catalytic activity regained by decreasing temperature. [21]

Coking means catalyst contamination with carbon-based residues. Formation of these residues takes place through complex secondary reactions after oxidation or decomposition of hydrocarbons. Coke causes deactivation through the geometric effect, as it blocks pores and active sites. Even 20% of the weight of a catalyst washcoat may be coke. [19]

3 X-ray photoelectron spectroscopy

3.1 Basic principles

X-ray photoelectron spectroscopy (XPS, or electron spectroscopy for chemical analysis, ESCA) is an experimental, non-destructive method for chemical characterization of solid surfaces. It is based on the photoelectric effect and counting electrons of different kinetic energy. The method can be used for identifying chemical compounds on a sample surface qualitatively and determining atomic concentrations quantitatively.

In the photoelectric effect, electron emission from an atom occurs when the atom absorbs a photon of energy $h\nu$. The energy freed in the photon absorption is consumed by an electron according to the equation

$$h\nu = W + K_{\max}. \tag{8}$$

W is the work needed to dislocate the electron from its shell and $K_{\max}$ is the kinetic energy the electron gains thereafter. If $h\nu$ does not exceed W the photoelectric effect cannot take place. Thus, the energy of one photon must be high enough (or wavelength short enough). Hence, increasing intensity of the radiation (i.e. photon count) can only increase the intensity of electron emission but the occurrence of photoelectric effect does not depend on it at all.

Binding energy is the energy difference between a bound electron state and Fermi level. Using the definition, equation 8 can be rearranged as

$$E_b = h\nu - K_{\max} - \phi, \tag{9}$$

where ϕ is a analyzer-dependent workfunction, known for a given measurement system [24]. In an XPS measurement, the incident photon energy is also known, and the kinetic energy of an electron is the observable actually being measured. Thus, binding energy of a single electron can be calculated. The initial result of any XPS measurement is a spectrum plotting number of emitted electrons (photoelectrons) as a function of their binding energy. Figure 4 summarizes the essential parts of an XPS measurement. More technical details of X-ray production and electron detection are discussed in section 4.1.

3.2 Interpretation of photoelectron spectra

Figure 5 shows a general XPS spectrum (of a HPW treated catalyst sample C3, see section 4.2 for further information). The binding energy range from

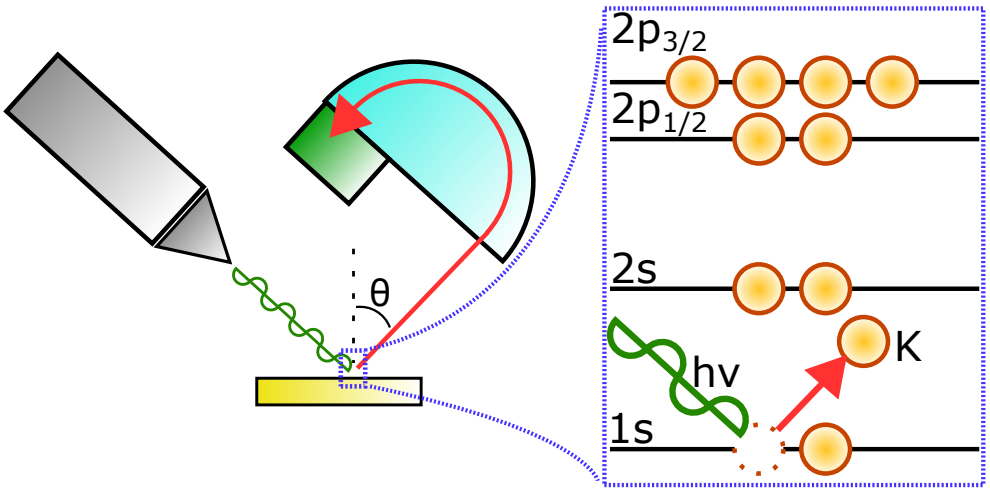

Figure 4: A schematic illustration of the X-ray photoemission process and geometry

0 to 1000 eV is usually enough to detect any element in the sample. The electron intensity is directly proportional to the actual number of electrons but depends also on measurement electronics and is thus always expressed in arbitrary units. The energy axis conventionally shows increase of kinetic energy and hence the binding energy decreases from left to right.

Each chemical element, except hydrogen and helium that are not easily detected in XPS, produces a characteristic set of local maxima in an XPS spectrum. These sets of binding energy values are widely tabulated and readily available in literature. Every element gives rise to multiple peaks since electrons originating from different shells have different binding energies. These spectroscopic core states are governed by quantum numbers $n = 1, 2, ...,$ $l = 0, 1, ..., n-1$ and $j = |l \pm s|$, where $s = \frac{1}{2}$. A conventional way for denoting each photoelectrons and XPS peaks for a given element A is "A nl_j", where l is denoted with letters s = 0, p = 1 and so on. In general, the lower the core state of the electron is, the higher its binding energy is. When $l = 0$ the spin-orbit coupling does not produce split states, but in other cases there are always two spectroscopic states for each pair of n and l. For two peaks with different n or l binding energy separation is usually in the range of tens to hundreds of electron volts. For a system of two peaks with same n and l but different j, often called a doublet, the separation is usually less than 10 eV. Sometimes the two peaks in such a doublet are in fact too close to be distinguished (separation $<$ 1 eV). For instance, this is the case with sulfur

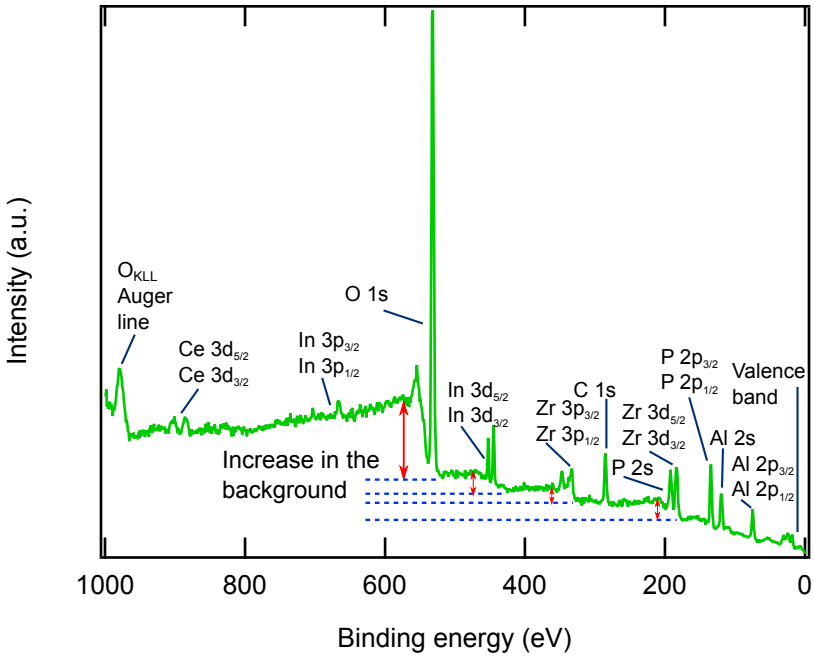

Figure 5: A typical XPS spectrum showing a binding energy range from 0 to 1000 eV.

2p, as can be seen in section 5. The degeneracy of one nl_j state is $2j + 1$, which gives all doublets characteristic intensity ratios. [24]

As figure 5 shows, the XPS spectra do not look ideal. In addition to sharp photoemission lines there are other features as well. Perhaps most notably, there is a background that rises almost stepwise on the left hand side of every major peak. This is due to electrons that originate from atoms below the surface. They experience inelastic scattering before reaching the vacuum thus losing their kinetic energy (hence the subscript 'max' in equations 8 and 9). Since they enter the detector with a reduced kinetic energy, by equation 9 they appear in the spectrum at higher binding energy than they initially had.

There are also additional peaks in an XPS spectrum. Plasmon peaks originate from inelastic energy losses where photoelectrons excite modes of collective oscillation of conduction electrons in a metal bulk. Due to the discrete nature of oscillation frequencies, the photoelectrons lose discrete values of energy, and peaks instead of a constant background is formed in the spectrum. Auger peaks appear as a result of secondary emissions. Auger process is a way to de-excitate an ionized atom after photoemission. An electron of a higher

state fills a void left in a lower state by the photoelectron. A third electron acquires the energy freed in this transition as its kinetic energy, leaving the ion, simultaneously increasing its charge number further by one. Moreover, X-ray photons with different characteristic energies ($h\nu$) cause satellite peaks to appear in a constant distance from main peaks, again by equation 9, if the X-ray source is not monochromatic. Shake-up satellites appear when a part of the photon energy is consumed by exciting an electron to a higher level thus leaving the photoelectron with less kinetic energy. The peaks at a very low binding energies form the so-called valence band. The photoelectrons contributing to it originate from molecules and have a strongly covalent nature. [24]

Every photoelecton peak has a non-zero width and thus slight variation in the binding energy. This comes from properties of the analyzer used, variations of photon energy and the uncertainty principle $\Delta E = \frac{h}{\tau}$, where h is Planck's constant and τ is lifetime of an empty state in an ion, i.e. the time interval between photoemission and a decay, the Auger process for instance [24]. Due to these deviations, XPS lines generally have a symmetric peak form. The width is usually expressed as the full width at half maximum (FWHM) which means the total width at the averaged intensity of the maximum intensity and the background level [24].

3.3 Line intensities and elemental composition

One of the main results XPS is able to give is the elemental composition of the measured sample, i.e. the relative atomic concentration of each element. The number of atoms of a given element is linearly proportional to the intensity of any of the photoelectron peaks, although the relation is not trivial. The following is a greatly simplified explanation how atomic percentages are acquired. A given amount of an element A on the sample surface gives a peak of intensity I_0. Several factors contribute to I_0 and it can be written [25]

$$I_0 = K\sigma_{\mathrm{A}}C_{\mathrm{A}}. \tag{10}$$

Here, C_{A} is the absolute atomic concentration of element A (as atoms per unit volume) and σ_{A} is the photoemission cross-section expressing the probability for the particular photon to cause an emission of an electron from the particular shell. K incorporates many parametres characteristic to the experimental set-up geometry, optics and electronics. They are not necessarily even known but can be considered constant within a given experimental set-up regardless what is being measured.

If the same amount of element A is not on the surface, but under a layer of thickness t, the intensity will be attenuated as

$$I_t = I_0 \exp\left(\frac{-t}{\lambda_\mathrm{A} \cos\theta}\right), \tag{11}$$

where λ_A is an inelastic mean free path (IMFP) of the electron [24]. It means the average distance the electron can travel within the solid sample without experiencing inelastic collisions [25]. Its value depends on the atom and the shell. θ is the detection angle as shown in figure 4. There is a decay in the signal intensity as t increases. This is because the probability for an inelastic collision increases, and some of the electrons only contribute to the inelastic background while some cannot even escape the sample bulk. Because of this, XPS is a surface sensitive method, with information depth ranging from 5 to 15 nm, depending on the transitions measured [24].

For a sample of finite thickness t, the intensity of element A is naturally an integral over the bulk, and with equations 10 and 11 it can be written as [26]

$$I_\mathrm{A} = K \sigma_\mathrm{A} C_\mathrm{A} \int_0^t \exp\left(\frac{-z}{\lambda_\mathrm{A} \cos\theta}\right) \mathrm{d}z. \tag{12}$$

If the sample is homogenous for the whole information depth it is justified to regard it as a semi-infinite slab, setting $t \to \infty$ [24]. After integration and substitution the intensity is $I_\mathrm{A} = K \sigma_\mathrm{A} C_\mathrm{A} \lambda_\mathrm{A} \cos\theta$. The unknown K is still there, but given the assumption that it does not change with energy, it cancels out when a relative atomic concentration, i.e. C_A divided by concentrations of all elements, is calculated, giving

$$c_\mathrm{A} = \frac{C_\mathrm{A}}{\sum_i C_i} = \frac{I_\mathrm{A} \sigma_\mathrm{A}^{-1} \lambda_\mathrm{A}^{-1}}{\sum_i I_i \sigma_i^{-1} \lambda_i^{-1}}. \tag{13}$$

Therefore, in order to gain elemental composition only intensities, photoemission cross sections and IMFPs are required. Intensities are being measured and IMFPs and cross sections can be determined with a use of tabulated values and empirical formulas as illustrated in figure 6. Photoemission cross sections have been derived from experimental results and calculated [27]. They are also known as Scofield factors. IMFP values can often be approximated adequately enough as a rising function of electron kinetic energy. In this work, they were estimated with the equation

$$\lambda = \left(\frac{h\nu - E_b}{h\nu - E_\mathrm{C1s}}\right)^{0.7}, \tag{14}$$

provided by the manufacturer of the equipment. Here, E_{C1s} is the binding energy of 1s line of adventitious carbon.

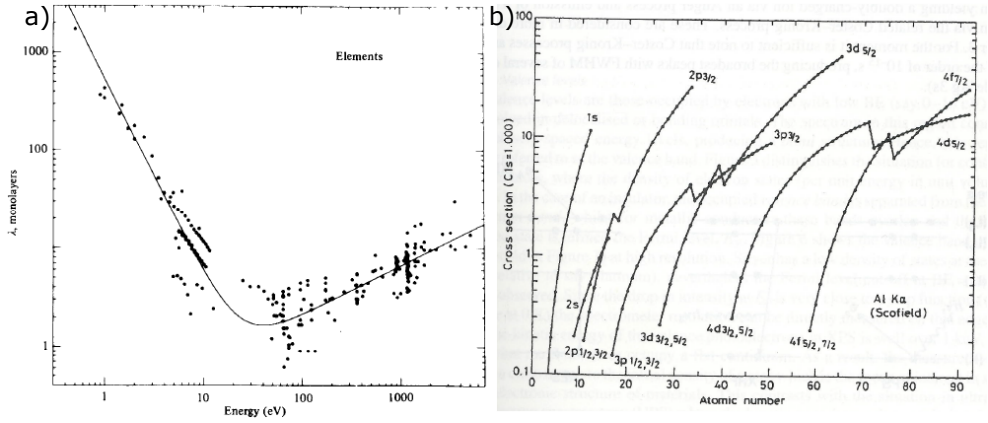

Figure 6: (a) IMFP values as a function of photoelectron kinetic energy. Copyright 1979 John Wiley and Sons. Reproduced with permission from Reference [28]. (b) Photoemission cross sections as a function of atomic number [24, 27]. Copyright 2003 IM Publications and SurfaceSpectra Ltd. Reproduced with permission from Reference [24].

3.4 Chemical shifts

An essential feature in XPS is the possibility to distinguish different chemical states and molecules based on small shifts in binding energy values of the photoelectron peaks. These shifts occur due to different oxidation states and different chemical environments. According to electrostatic charge potential model, a three-term expression for the shift of an arbitrary photoelectron peak of element A can be written as

$$\Delta E_b = \frac{\Delta q_A}{r_V} - \frac{\sum_i \Delta q_{Ai}}{r_{Ai}} - \Delta R. \tag{15}$$

Here, the first term represents change in valence charge with an averaged valence orbital radius. The second term represents potentials at the atom caused by surrounding atoms. The final term is a relaxation term, describing how the atom and surroundings react to the empty state created by photoemission. The terms may also cancel each others resulting in fairly small shifts. [25]

The chemical shifts are usually in the range of several electron volts, roughly

up to 10 eV. In general, bonding to electronegative atoms increases the binding energy of the atom A [24]. As a consequence of this, for instance metal oxides produce XPS peaks of higher E_b than corresponding metallic states do. Binding energy shifts, like elemental XPS line sets, are well tabulated and widely available. Therefore it is often sufficient to compare acquired results with literature in order to determine chemical states.

3.5 Numerical analysis of XPS spectra

In order to calculate atomic concentrations, it is required to distinguish peaks from the background. As figure 5 shows the inelastic background rises almost stepwise at each photoelectron peak. A question arises how the background behaves directly under the peak, or at what intensity the background ends and the actual peak begins. There are several background subtraction methods widely in use. In this work, iterative Shirley method is applied. The Shirley background is subtracted from an experimental spectrum $j(E)$ as

$$F_{k+1}(E) = j(E) - j(E_{\min}) \frac{\int_E^{E_{\max}} F_k(T) \mathrm{d}T}{\int_{E_{\min}}^{E_{\max}} F_k(T) \mathrm{d}T}, \tag{16}$$

where F_k is the background-corrected spectrum after k iterations [29, 30]. The itaration is carried on until the changes are below a threshold value. Beside the original spectrum, the only parametres needed in the process are the endpoints $E_{\min}$ and $E_{\max}$.

Another option for background subtraction is Tougaard method. It is based on the theory of electron scattering and can thus provide physically more accurate background levels than the Shirley method which is empirical [31]. On the other hand, the most straightforward way, linear subtraction can also give adequate results depending on the initial spectra. The Shirley subtraction was chosen for this work since it is widely used and has been found to produce reasonable spectra in many cases. The way how the endpoints are chosen may or may not have a strong effect on the produced background. In general, if the peak intensity is high the background stays relatively similar even if endpoints are changed for several electron volts. On the other hand, if the peak intensity is in the same order of magnitude with the noise level in the background, as often is the case, a slight change in endpoints can have an enormous impact on the background. In those situations there is a need to make the choice in such a way that the background looks reasonable.

As mentioned before, the XPS lines have a non-zero width. Therefore, it is

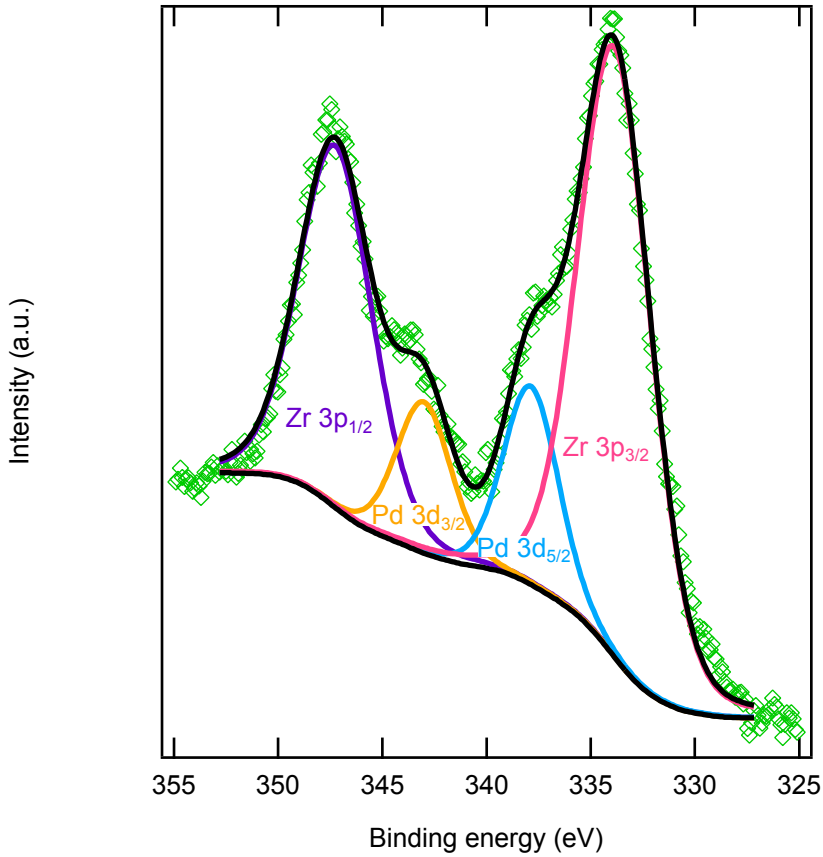

Figure 7: A spectrum with four photoelectron peaks. Shirley background subtraction and Lorentzian-Gaussian peak fitting have been applied.

sufficient to interpret the intensities I_0, I_t and I_A in equations 10-13 as the intensity maxima of measured peaks only when all the considered peaks have equal width and none of them overlap. In many cases however, these conditions are not met. Then, it is required to consider peak areas instead, as they describe the total intensity of the given electron core states much more accurately. Thus, the area between the measured data and the subtracted background needs to be calculated. The simplest way to do this is of course numerical integration, where the area can be computed point-by-point using for instance the midpoint rule. However, in cases where two or more peaks overlap, the contribution of each peak needs to be deconvoluted and direct integration cannot be used. Instead, the areas can be calculated by fitting a theoretical curve in the measured data. The contribution of the finite average lifetime of a hole state gives rise to a Lorentzian peak form [32]. The Lorentz

function can be written as

$$L(E) = h\left[1 + \left(\frac{E_0 - E}{\beta}\right)^2\right]^{-1}, \tag{17}$$

where E_0 is the centroid energy of the peak, h is the height of the calculated peak and β is a width parameter, ca. one half of the FWHM value [30]. Photonic and analyzer-related widening in photoelectron peaks are Gaussian by nature [24]. The Gauss function is

$$G(E) = h\exp\left[-\ln 2\left(\frac{E_0 - E}{\beta}\right)^2\right]. \tag{18}$$

Therefore, the fitting function needs to be a convolution of these two peak forms, called Voigt function [30]. When fitting a single-peak spectrum, there are four free parametres, E_0, h, β and a biasing parametre for giving more weight for either the Lorentzian or Gaussian peak form. Fitting multiple peaks is otherwise similar, but the fitting parametres of each peak may not always be independent. For example, two peaks originating from different chemical states are bound to have the same FWHM. The fitting itself means minimization of the chi-square value

$$\chi^2 = \frac{1}{p-n}\sum_{i=0}^{p}\left(\frac{F_i - \hat{F}_i}{\sigma_i}\right)^2, \tag{19}$$

where p is the number of data points and n is the number of free parametres. F_i and $\hat{F}_i$ are the data and fit values at point i, respectively [31]. The standard deviation $\sigma_i = \sqrt{F_i}$ since photoelectron detection follows Poissonian statistics [31]. Figure 7 shows an example of four-peak spectrum with a subtracted Shirley background and deconvoluted Lorentzian-Gaussian peaks.

The binding energy of a peak is in general the value where the intensity is at maximum. If fitting is applied, then the centroid energy E_0 can naturally be considered the binding energy. However, for various reasons the binding energy scale can systematically have an offset of several electron volts. Therefore, a peak with a known binding energy value needs to be used as a reference and all others calibrated using the same offset. Adventitious carbon 1s line is a conventionally used reference.

4 Experimental details

4.1 The measurement setup

The XPS measurements described in this work were carried out with Surface Science Laboratories SSX-100 system. It features an X-ray radiation source, equipped with an aluminum anode. When bombarded with electrons of energy of 10 keV, the anode emits characteristic Al K_α X-ray photons, with a photon energy of 1486.6 eV. In addition, the acceleration of electron towards the anode also gives rise to less prominent characteristic photons and a continuous spectrum of bremstrahlung photons. Therefore, the measurement system is equipped with a quartz crystal monochromator that filters out the undesired wavelengths. This way, the unwanted satellite peaks in a spectrum can be avoided. The X-ray gun is capable of producing spot sizes from 200 to 800 micrometres.

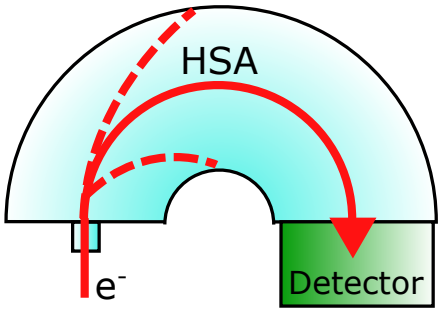

Figure 8: A schematic illustration of the working principle of a hemispherical sector analyzer.

A fraction of the photoelectrons emitted from the sample surface are first focused by a lens and then collected by a hemispherical analyzer (figure 8). The analyzer has radial metal plates with an adjustable potential difference ΔV producing an electric field of magnitude E. The electric field forces an electron to adopt a circular path of radius r, where the relation between the field and radius is

$$eE = m_e \frac{v^2}{r}, \tag{20}$$

where e is elementary charge, m_e the mass of an electron and v its speed. Hence, a given value for ΔV allows only electrons with certain velocity and therefore certain kinetic energy (pass energy) to pass through the analyzer. Controlling ΔV thus enables measurements of a desired kinetic energy range,

or by equation 9, a binding energy range. From the analyzer the electrons proceed to a detector that counts their number for each of the measured binding energy ranges. Thus, when ΔV is altered systematically, the number of electrons can be expressed as a function of kinetic, or binding energy. The signal given by the detector is then amplified, and the detection line is connected to a computer through which all operations and data are maintained.

The emission of photoelectrons ionizes surface atoms of a non-conductive sample thus electrically charging it. To neutralize this effect, the system is equipped with an electron flood gun that produces a constant electron beam targeting the sample. Electrons with low energy, typically less than 1 eV thus compensate the electron loss occuring during the photoelectric effect. In addition, using sample holders of conductive material helps in avoiding charging and thus improves quality of the acquired spectra.

XPS measurements require high vacuum conditions ($\leq 5 \times 10^{-7}$ mbar), as the photoelectrons cannot travel from the sample surface into the analyzer in an excess of gas-phase particles without collisions. The system features two chambers, a main chamber for measurements, and a load-lock for sample introduction and storage. The main chamber has a base pressure of 5×10^{-10} mbar which is maintained with a cryogenic sorption pump and an ion pump. The load-lock is pumped with a turbomolecular pump and it is able to reach a pressure of 10^{-6} mbar or less. The two chambers are separated with a gate valve, and the main chamber does not need to be exposed to pressures higher than the lowest possible load-lock pressure during any normal operation.

4.2 Catalyst samples and aging treatments

The catalysts studied in this work are prototypes of commercial solutions for natural gas and diesel oxidation. All of them were manufactured by Dinex Ecocat Oy. The laboratory-aged and then measured samples were pieces of the honeycomb used in the actual converters. The materials of the catalyst samples and their intended use are listed in table 1. In addition to the actual catalysts, samples of a bare supporting washcoat lacking the catalytically active noble metals were studied as well. This provided a way to examine the role of the active particles in the deactivation processes.

The samples were subjected to laboratory-scale aging treatments simulating real-life conditions in an engine. All the treatments are listed in table 2. However, every treatment was not applied to every sample. Thermal aging, carried out in Tampere University of Technology, was done in several tem-

Table 1: A list of catalyst and support samples studied in this work.

Ref.	Description	Active metal	Support	Additive oxides
C1	A high-loading catalyst for natural gas oxidation	Pt, Pd (1:4)	Al_2O_3	-
S1	The washcoat for C1 without noble metals	-	Al_2O_3	-
C2	A high-loading catalyst for natural gas oxidation	Pt, Pd (1:4)	Al_2O_3	Ce, Zr
C3	A low-loading catalyst for diesel oxidation	Pt, Pd (4:1)	Al_2O_3	Ce, Zr, Si, Ti
C4	A low-loading catalyst for diesel oxidation, similar to C3 but does not contain palladium	Pt	Al_2O_3	Ce, Zr, Si, Ti
S3/4	The washcoat for C3 and C4 without noble metals	-	Al_2O_3	Ce, Zr, Si, Ti
C5	A low-loading catalyst for diesel oxidation	Pt	SiO_2, ZrO_2	-
S5	The washcoat for C5 without platinum	-	SiO_2, ZrO_2	-

peratures ranging from 700 °C to 1100 °C in a minimal gas flow. All other treatments (done in University of Oulu) were carried out in a tubular quartz reactor at 400 °C with a gas mixture flow rate of 1 $\frac{\text{l}}{\text{min}}$. Before the treatments, the reactor was heated up to 400 °C using a gas mixture of air (10%) and N_2 (90%). Each treatment lasted for 5 hours and in all cases the gas mixture was balanced with nitrogen. Sulfur dioxide and ammonium phosphate were used as precursors for sulfur and phosphorus poisoning, respectively.

This work concentrates on the results acquired in XPS measurements carried out in Aalto University. In addition, several other methods, such as transmission electron microscopy (TEM) and activity tests, have been in use to study the same set of catalyst samples. That work has been done in University of Oulu and Tampere University of Technology. Some main results of those

Table 2: A list of the aging treatments carried out for the measured samples.

Ref.	Description	Gas mixture
fresh	As-received	
W	Hydrothermal aging	10% H_2O, 10% air, 80% N_2
S	Sulfur poisoning without water	100 ppm SO_2, 10% air, ca. 90% N_2
SW	Sulfur poisoning with water	100 ppm SO_2, 10% H_2O, 10% air, ca. 80% N_2
LPW	Phosphorus poisoning, low phosphorus concentration	10% H_2O with 0.065 $\frac{mol}{l}$ $(NH_4)_2HPO_4$, 10% air, ca. 80% N_2
HPW	Phosphorus poisoning, high phosphorus concentration	10% H_2O with 0.13 $\frac{mol}{l}$ $(NH_4)_2HPO_4$, 10% air, ca. 80% N_2
PSW	Phosphorus-sulfur poisoning	100 ppm SO_2, 10% H_2O with 0.13 $\frac{mol}{l}$ $(NH_4)_2HPO_4$, 10% air, ca. 80% N_2
TA	Thermal aging	20% O_2, 80% N_2

studies are summarized in chapter 6.

4.3 Sample preparation and measurements

Prior to the XPS measurements the catalyst samples needed to be prepared. A solid piece of the catalyst honeycomb was unsuitable to be measured as such, since the relatively thick layer of the non-conductive washcoat would have caused charging during the measurement. Therefore, small amount of catalyst powder on the honeycomb surface was scraped off and pressed against an indium film in order to have a thinner non-conductive layer and thus to diminish the charging effect. Indium as a metal is conductive, but it is also soft and therefore a well-suited and firm stage for powder. In addition, the electron flood gun was used with an energy of roughly 0.1 eV throughout the measurements to further compensate charging. The first 5 mm from each end of the treated catalyst samples were used for scraping in order to do separate XPS measurements for inlet and outlet sections.

The measurements with the SSX-100 system were controlled with a computer through ESCA2005 software. With every new sample, a general spectrum of binding energies from 0 to 1000 eV was measured first. Monitoring the relative indium line intensities gave some idea how catalyst-rich the measured area was. Moreover, the relative intensity for carbon 1s line showed how much adventitious carbon the surface contained, i.e. how clean it was. All the interesting regions where then measured one by one. Measurement time depended strongly on how well the line could be detected. The number of scans needed to acquire a decent enough spectrum showing the desired features varied from five to three hundred. A typical measurement window was 20 eV, but for doublets for instance, a wider range was needed. The used spot size was typically 600 µm although 800 µm was used in some cases as well. As an example, figure 9 shows the general spectra of two measured samples.

None of the treatments in table 2 involved carbon in the process. Therefore it can be concluded that carbon detected on the sample surface is adventitious carbon, which is conventionally used as an origin when determining binding energy offset [24]. Several values for binding energy of C 1s line of adventitious carbon are given in literature [33], and the one that has been used here is 284.6 eV. In order to use C 1s as a reference, the region was measured although the contribution of carbon was then excluded from the compositional analysis. As mentioned before, Shirley background subtraction and Lorentzian-Gaussian peak fitting were applied. The peak form was dominantly Gaussian with 80% weight.

In all measurements (except for the general spectra) an energy step size of 0.1 eV was used, thus setting an ultimate lower limit for binding energy accuracy. In practice, when adventitious carbon is used as a reference, the accuracy is ± 0.5 eV at best [24]. This can be considered a reasonable limit of error in binding energy for those elements that have atomic concentration of 1% or more. For elements with lower content the measured data usually has a relatively poor signal-to-noise ratio. Therefore, larger error bars need to be applied. As a rough estimate, the peak centre can often be determined with accuracy of 0.5 eV, and when the contribution of carbon is taken into account, this gives ± 1.0 eV for limits of error.

The way the background is chosen and the fit is made can cause alterations to atomic percentages. In general, XPS can provide a 90% accuracy for the atomic concentration of major elements. This can be assumed in this work as well. Accuracy is discussed further in section 5.4.

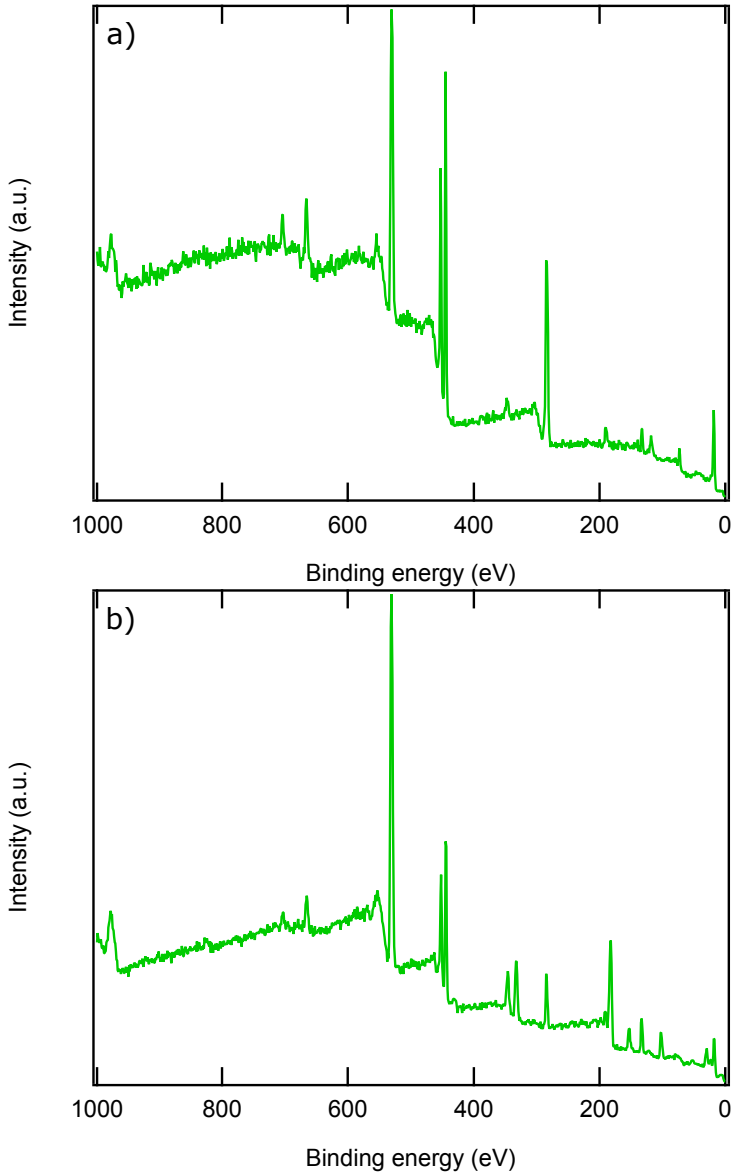

Figure 9: a) A general spectrum of an LPW treated S1 catalyst sample. The features are similar to C3 (figure 5) but many peaks are missing due to the simpler chemistry. b) A general spectrum of an HPW treated C5 catalyst sample. Silicon peaks are visible around 100 and 150 eV.

5 Results

5.1 Alumina supported platinum and palladium catalysts for natural gas oxidation

5.1.1 Effect of phosphorus poisoning

Natural gas oxidation catalyst samples C1 and C2 were subjected to phosphorus poisoning using both the weaker (LPW) and the stronger (HPW) phosphorus solutions. In addition, also the bare washcoat S1 was treated similarly. P 2s peaks were measured from the inlet and outlet ends of the treated samples to observe the accumulation of phosphorus. Figure 10 shows the phosphorus spectra measured from the inlet sides. The outlet side spectra are qualitatively similar. As seen in table 3, the binding energy value of a P 2s peak was in all cases within a range of 190.9-191.9 eV. This suggests that phosphorus is on the catalytic surface as phosphate [34].

Table 4 shows the measured atomic percentages of each element in the phosphorus poisoned samples and also reference values measured in fresh samples. The atomic percentage of phosphorus varies quite largely, from 0.2 to 12%.

Table 3: Binding energy values (in eV) of the major XPS lines measured from the fresh and phosphorus poisoned NGO catalyst samples.

			Pt $4d_{5/2}$	Pd $3d_{5/2}$	P 2s	Al 2s	O 1s
Pt-Pd catalyst (C1)	fresh		315.3	336.3	-	118.3	530.2
	LPW	in	315.7	337.0	191.2	119.1	531.2
		out	315.7	337.4	191.9	119.7	531.7
	HPW	in	315.3	336.7	190.9	118.7	531.4
		out	314.7	336.4	190.9	118.5	530.8
Pt-Pd catalyst (C2)	fresh		315.1	336.7	-	119.1	530.9
	LPW	in	315.0	337.2	191.6	119.5	531.4
		out	315.4	336.5	191.2	118.8	530.7
	HPW	in	315.0	336.7	191.1	119.0	530.9
		out	314.7	336.7	190.9	118.8	530.9
Support (S1)	fresh		-	-	-	118.7	530.9
	LPW	in	-	-	191.3	119.1	531.8
		out	-	-	191.1	118.8	531.2
	HPW	in	-	-	191.8	119.5	532.0
		out	-	-	191.5	119.2	531.8

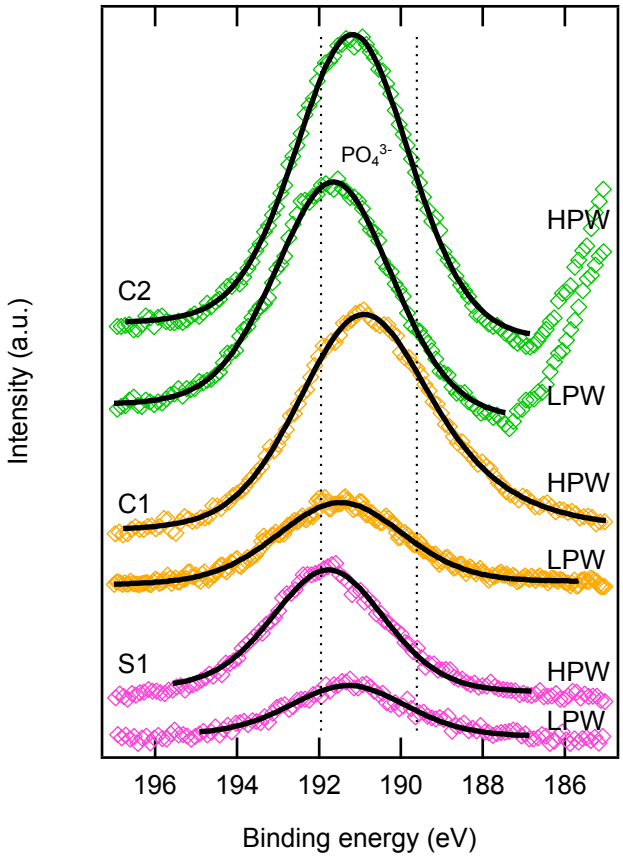

Figure 10: Phosphorus 2s peaks measured from the inlet side of samples C1, C2 and S1. Phosphorus appears on the sample surfaces as phosphate.

Based on the results, phosphorus seems to strongly prefer adsorption on the inlet end, which is evident in all the samples. HPW poisoning resulted in slightly higher phosphorus content than LPW treatment did. In the inlet, the atomic percentages of phosphorus in LPW treated samples were ca. 80% of those of HPW treated ones. However, a similar trend was not observed in outlet measurements.

In the fresh samples C1 and C2 the atomic percentage of platinum was 0.08% and 0.07%, respectively. As shown in table 4, significantly smaller concentrations were detected in the phosphorus treated samples, especially in C1. Figure 11a) shows the Pt $4d_{5/2}$ spectra in the fresh and the inlet ends of the phosphorus poisoned samples. The Pt spectrum taken from the LPW treated sample has been scaled so that the peak form would be visible. Only a very slight amount of platinum was found in that sample. However, it must

Table 4: Elemental compositions (in at.%) measured from the fresh and phosphorus poisoned NGO catalyst samples.

			Pt	Pd	P	Al	O	Ce	Zr
Pt-Pd catalyst (C1)	fresh		0.08	0.39	-	36	64	-	-
	LPW	in	0.01	0.26	6.6	28	65	-	-
		out	0.01	0.25	2.9	35	62	-	-
	HPW	in	0.04	0.35	7.8	26	66	-	-
		out	0.03	0.33	0.23	36	63	-	-
Pt-Pd catalyst (C2)	fresh		0.07	0.47	-	28	66	0.71	4.9
	LPW	in	0.03	0.28	10	16	71	0.36	2.8
		out	0.03	0.39	4.9	25	69	0.45	3.6
	HPW	in	0.04	0.32	12	17	68	0.34	3.9
		out	0.04	0.33	2.1	27	66	0.52	3.9
Support (S1)	fresh		-	-	-	34	66	-	-
	LPW	in	-	-	8.4	11	80	-	-
		out	-	-	5.7	27	68	-	-
	HPW	in	-	-	11	20	68	-	-
		out	-	-	5.8	22	72	-	-

be remembered that the mere peak intensity is not enough for determining atomic concentration, as all peaks in one measurement may have relatively low intensity for various reasons. The binding energy for Pt $4d_{5/2}$ was found to be 315.3 eV and 315.1 eV in the fresh samples C1 and C2, and between 314.7 and 315.7 eV in the phosphorus treated samples. These values suggest platinum being most likely as oxide in all cases. The gained values most strongly refer to PtO for which binding energies between 314.7 and 317.3 eV have been reported [34, 35]. The values below 315 eV may also indicate reduction to metallic platinum, but since they were observed in outlets, where poisoning effect can be assumed to be weaker, the deviation is probably not a sign of chemical changes.

Pd 3d regions of the fresh and P treated (inlet) samples are shown in figure 11b). The figure includes both $3d_{5/2}$ and $3d_{3/2}$ peaks although only the contribution from the stronger $3d_{5/2}$ peaks has been included in the analysis. In sample C2, the 3p peaks of zirconium are in the same binding energy range which complicates extracting palladium peaks from the experimental data (see the earlier figure 7). According to table 3 the binding energy of Pd $3d_{5/2}$ is 336.3 and 337.3 eV in the fresh catalyst samples and ranging from 336.4 to 337.4 eV in the poisoned samples. Palladium is clearly oxidized, and fur-

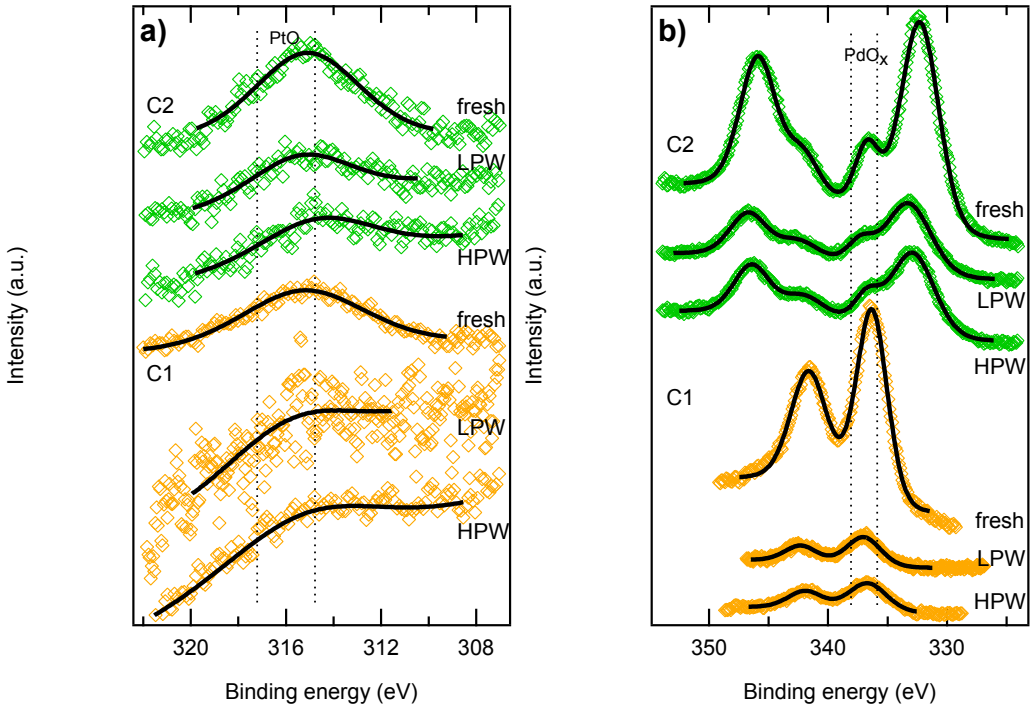

Figure 11: (a) Platinum $4d_{5/2}$ and (b) palladium 3d peaks measured from the inlet side of phosphorus poisoned samples C1 and C2. Both noble metals are in an oxidized form.

thermore it is obvious that reduction does not take place due to phosphorus contamination. Palladium is probably as PdO, but also a mixed oxide with higher oxidation states is possible [34, 36]. As with platinum, the atomic concentration of palladium is observed to have decreased in the treated samples, although the relative loss is not as drastic.

Elements in the washcoat did not show significant changes due to phosphorus poisoning. Some variation in binding energy did occur, as table 3 shows, but the fairly small differences do not suggest changes in chemical state. Cerium and zirconium, the additives in catalyst C2 have not been included in the binding energy table. Both were observed as oxides. Also the atomic percentages showed only slight variations.

5.1.2 Effect of thermal aging and sulfur poisoning

A series of combined chemical and thermal treatments were performed to the catalyst C1. The catalyst was exposed to sulfur poisoning (SW) and thermal

aging (TA) in three different temperatures (700, 1000 and 1100 °C). A sample aged at 1000 °C was treated with sulfur thereafter (TA + SW), and vice versa, a sulfur poisoned sample was thermally aged at 1000 °C (SW + TA).

In addition, a sample undergone thermal aging at 1000 °C, sulfur poisoning and an activity test was also measured with XPS. In the activity test the catalyst is kept in a flow reactor. A constant feed of a gas mixture simulating real exhaust gas composition travels through the reactor. The amount of gaseous components is monitored and conversion rates calculated. The laboratory gas mixture used for simulating natural gas is 600 ppm CH_4, 500 ppm CO, 10% CO_2, 12% O_2 and 10% H_2O balanced with N_2.

In this series of XPS measurements the samples were not measured separately in outlet and inlet ends since earlier studies with other methods suggested there would be no significant differences. Moreover, the thermal aging was carried out with almost zero gas flow. Since all photoelectron peaks were either clearly and unambiguously visible or not detectable at all, peak fitting was omitted in the atomic percentage calculation process and direct integration was used instead.

Figure 12 and table 5 show that binding energies of S 2p peaks vary from 168.5 to 169.7 eV. This indicates that sulfur occurs as sulfate molecules [36] similarly to what has earlier been found after S poisoning treatments. Based on atomic percentages in table 6 thermal aging before sulfur poisoning has had no clear effect on accumulation of sulfur. On the other hand, hardly any sulfur was detected in the SW + TA treated sample. Therefore, sulfur must either desorb from the surface or diffuse below it due to the thermal treatment.

Figure 13a) shows the Pt $4d_{5/2}$ spectra of a fresh and treated catalyst samples. In the sulfur poisoned sample platinum was found to appear as oxide [35]. An interesting feature is that platinum is virtually undetectable in all the thermally aged samples. The spectra thus suggest that structural changes take place during the heating process, leaving platinum below the surface.

Palladium 3d spectra are shown in figure 13b). Again, palladium probably appears as PdO or a mixed state [36]. However, a significant decrease in binding energy appears after the activity test. This indicates that palladium itself reduces to metallic during the exhaust gas oxidation. Part of the binding energy decrease may be due to calibration, as all peaks were found at lower binding energy after the activity test. The difference found in the palladium spectrum

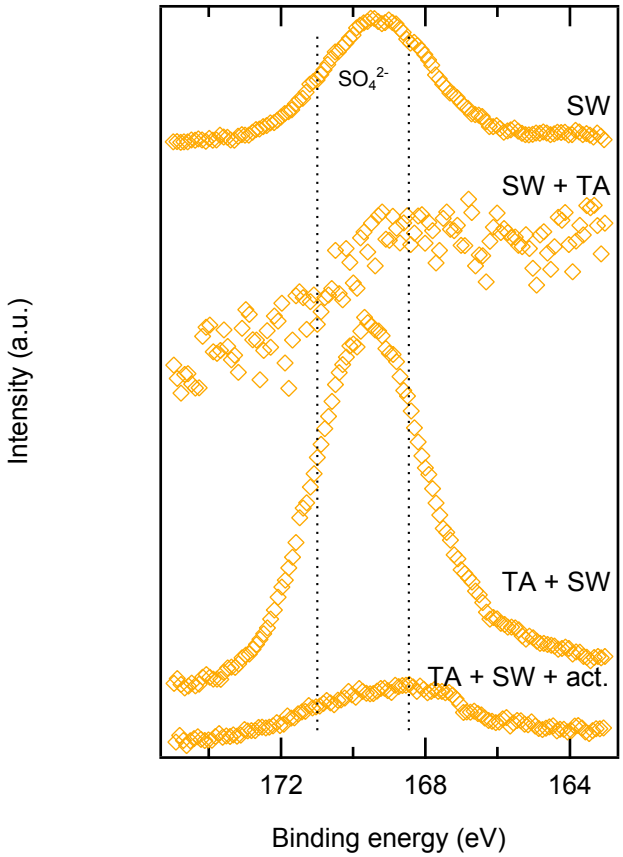

Figure 12: Sulfur 2p peaks of poisoned and thermally aged samples of C1. Sulfur occurs as sulfate. Thermal aging significantly decreases sulfur amount.

is however so large that it strongly suggests an actual change has occurred. Thermal treatment was seen to diminish palladium concentration, although not as strongly as platinum. Heating at 700 °C has had no apparent effect, but treatments at higher temperatures have significantly decreased palladium content on the surface, which again points towards structural changes. Aluminum and oxygen did not show any exceptional behaviour in any sample in the series.

Table 5: Binding energy values (in eV) of the major XPS lines measured from the fresh, sulfur poisoned and thermally aged NGO catalyst samples.

		Pt $4d_{5/2}$	Pd $3d_{5/2}$	S 2p	Al 2s	O 1s
Pt-Pd catalyst (C1)	fresh	315.3	336.3	-	118.3	530.2
	SW	315.5	336.8	169.5	119.3	531.2
	TA 700 °C	-	336.9	-	119.0	530.9
	TA 1000 °C	-	337.5	-	119.0	531.0
	TA 1100 °C	-	336.8	-	119.6	531.5
	SW + TA	-	337.2	169.2	119.0	531.1
	TA + SW	-	337.5	169.7	119.5	531.3
	TA + SW + act.	-	334.4	168.5	118.3	530.6

Table 6: Elemental compositions (in at.%) measured from the fresh, sulfur poisoned and thermally aged NGO catalyst samples.

		Pt	Pd	S	Al	O
Pt-Pd catalyst (C1)	fresh	0.08	0.39	-	36	64
	SW	0.07	0.27	2.4	34	63
	TA 700 °C	-	0.48	-	34	65
	TA 1000 °C	-	0.09	-	39	61
	TA 1100 °C	-	0.24	-	34	66
	SW + TA	-	0.07	0.3	38	62
	TA + SW	-	0.08	2.1	39	59
	TA + SW + act.	-	0.09	1.1	30	68

5.2 Alumina supported platinum and palladium catalysts for diesel oxidation

5.2.1 Effect of phosphorus poisoning

Diesel oxidation catalysts C3 and C4 were given phosphorus poisoning treatments (LPW and HPW). The catalysts are otherwise similar, but C3 has platinum and palladium as active metal whereas C4 has merely platinum. For reference, the same washcoat including neither noble metal (sample S3/4) was also given a HPW treatment.

Figure 14 shows the phosphorus spectra measured from the inlet ends. The spectra together with table 7 show that although there is some variation in the binding energy values, the phosphorus is clearly found to be phosphate

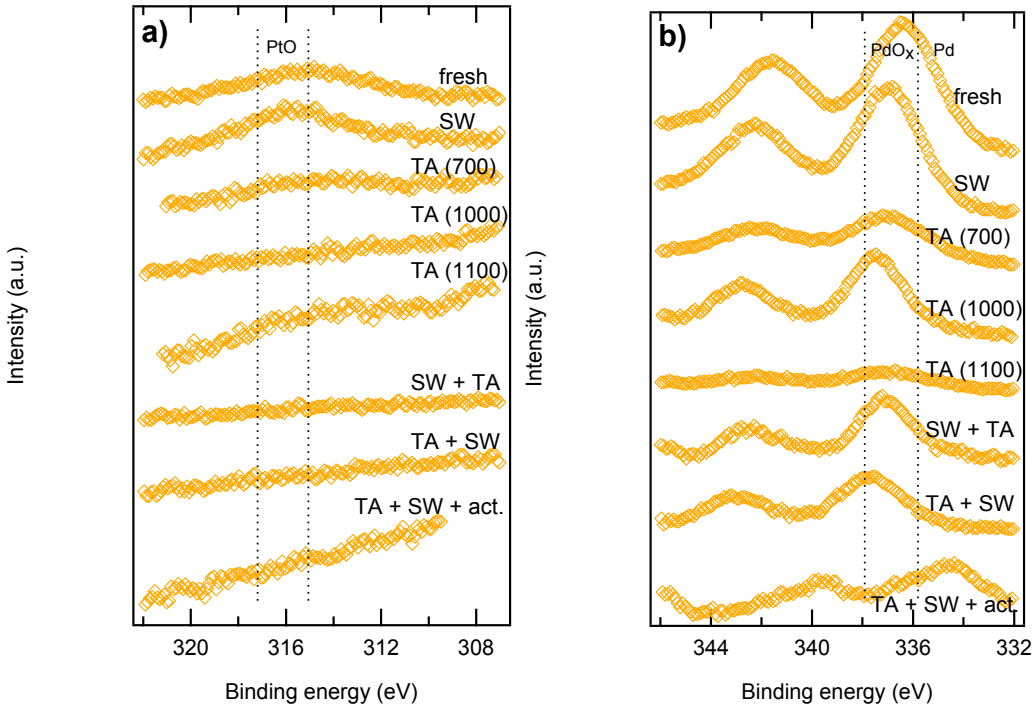

Figure 13: (a) Platinum $4d_{5/2}$ and (b) palladium 3d peaks measured from sulfur poisoned and/or thermally aged C1 samples.

in all samples [34]. Table 8 again shows the atomic concentrations of each element. In the NGO catalyst samples phosphorus selectively preferred adsorption on the inlet surface. This is not as clearly evident in this set of samples. Apart from the bare washcoat, larger concentrations of phosphorus were indeed observed in the inlet side measurements, but the differences are less significant than in the NGO catalysts. Differences between HPW and LPW treated samples are minimal as well. In fact, in C3 the LPW poisoning resulted in a larger phosphorus concentration. The small differences between the two ends and also between the HPW and LPW treated samples suggest that catalyst surfaces are nearly saturated with phosphorus.

The state of platinum was found to be strongly affected by the presence of palladium. As table 7 and figure 15a) show, Pt $4d_{5/2}$ lines peak at values between 315.0 and 315.5 eV in the C3 samples. Based on this, platinum is probably as PtO [34, 35]. Furthermore, there seem to be no changes in the chemical state triggered by the phosphorus treatments. In C4, however, the respective binding energy value for a fresh sample is 314.8 eV which can indicate metallic or oxidic form. The values measured in the treated samples

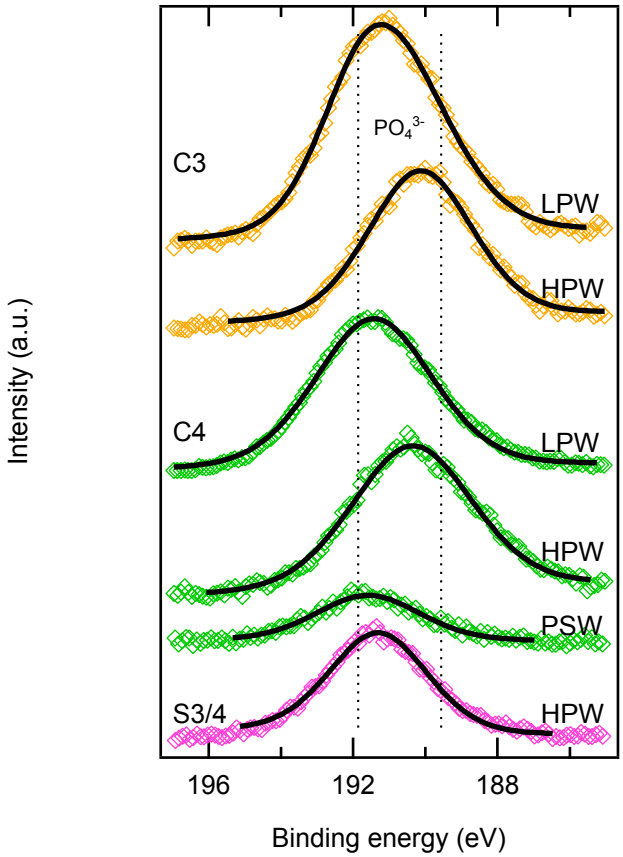

Figure 14: Phosphorus 2s peaks measured from the inlet side of samples C3, C4 and S3/4. Phosphorus appears on the sample surfaces as phosphate.

are significantly smaller indicating reduction to metallic platinum [35]. The difference between C3 and C4 is also obvious when it comes to atomic percentages of platinum. In C3, Pt concentration was found to decrease less than 50% in all treated samples. In C4, the decrease was more than 70% instead. In C3, the decrease in palladium was higher than in platinum, which indicates that phosphorus blocks less platinum sites when palladium sites are available, even though the decrease in their combined intensities was also less than 50%.

Palladium spectra are visible in figure 15b). They show Pd $3d_{5/2}$ peaks together with Zr $3p_{3/2}$ peaks. The binding energy range is from 336.3 to 337.3 eV, and no clearly changing trends are visible. Based on this, palladium appears as an oxide on the sample surface. It can be PdO or a mixed state [36]. Decrease in atomic percentage due to phosphorus treatment varies from 33 to 67 percent. However, in all samples the loss is larger than that of platinum.

Table 7: Binding energy values (in eV) of the major XPS lines measured from the fresh and phosphorus poisoned DOC samples.

			Pt $4d_{5/2}$	Pd $3d_{5/2}$	P 2s	Al 2s	O 1s
Pt-Pd catalyst (C3)	fresh		315.5	336.4	-	119.2	531.2
	LPW	in	315.4	337.3	191.2	119.2	531.4
		out	315.0	336.1	190.8	118.9	531.0
	HPW	in	315.0	336.9	190.1	118.1	530.8
		out	315.5	336.3	191.6	118.9	531.5
Pt catalyst (C4)	fresh		314.8	-	-	119.7	531.4
	LPW	in	314.2	-	191.4	119.2	530.3
		out	313.7	-	191.4	119.1	530.0
	HPW	in	313.2	-	190.4	118.2	530.3
		out	314.0	-	190.4	118.2	530.5
Support (S3/4)	fresh		-	-	-	119.1	531.2
	HPW	in	-	-	191.3	118.5	531.3
		out	-	-	191.2	118.8	531.4

This indicates palladium is more vulnerable to phosphorus poisoning.

Neither aluminum oxide nor the coating additives showed any interesting features. All of these elements maintain their atomic ratios and binding energies fairly consistently. Thus, XPS results do not suggest structural or chemical changes in the support.

5.2.2 Co-effect of phosphorus and sulfur

A sulfur poisoned (SW) sample of the catalyst C4 has been studied earlier. Sulfur was found to be as a part of a sulfate compound with atomic concentration of 2.5 percent. Platinum, with the binding energy of the $4d_{5/2}$ line at 314 eV, was found metallic. [37, 38]

Sulfur and phosphorus poisoning were combined in a simultaneous treatment (PSW). The spectra of phosphorus, platinum and sulfur are in figures 14, 15 and 16. According to the spectra and table 9, phosphorus appears again as phosphate and sulfur as sulfate. By table 10, phosphorus concentration in the inlet is one third smaller when compared to the HPW poisoned sample. The preference of phosphorus for sticking on inlet surfaces is evident again. In the SW poisoned sample, there were no difference in sulfur accumulation between inlet and outlet ends [37, 38]. Now, the percentage of sulfur atoms

Table 8: Elemental compositions (in at.%) measured from the fresh and phosphorus poisoned DOC samples.

			Pt	Pd	P	Al	O	Ce	Zr	Si	Ti
Pt-Pd catalyst (C3)	fresh		0.10	0.06	-	28	68	0.62	0.24	1.8	1.4
	LPW	in	0.08	0.02	7.3	19	69	0.40	0.26	4.1	0.83
		out	0.07	0.02	4.2	23	68	0.38	0.32	2.9	0.84
	HPW	in	0.07	0.04	5.6	22	68	0.39	0.28	3.5	0.66
		out	0.06	0.03	5.0	23	68	0.45	0.29	3.1	1.0
Pt catalyst (C4)	fresh		0.15	-	-	29	66	0.19	0.07	2.1	2.7
	LPW	in	0.03	-	5.0	23	66	0.12	0.10	3.2	2.0
		out	0.02	-	1.1	29	64	0.14	0.11	2.7	2.4
	HPW	in	0.04	-	6.1	22	67	0.16	0.14	3.9	0.89
		out	0.02	-	5.8	21	69	0.10	0.10	3.5	0.70
Support (S3/4)	fresh		-	-	-	26	70	0.18	0.05	1.5	1.7
	HPW	in	-	-	7.4	11	78	0.22	0.01	2.6	0.27
		out	-	-	12	10	75	0.16	0.05	2.7	0.69

doubles in the outlet. This suggests that phosphorus due to its selective behaviour dominates the adsorption on the inlet surface. In the outlet, there are more available sites for sulfur.

Table 9: Binding energy values (in eV) of the major XPS lines measured from the fresh and phosphorus-sulfur poisoned DOC samples.

			Pt $4d_{5/2}$	P 2s	S 2p	Al 2s	O 1s
Pt catalyst (C4)	fresh		314.8	-	-	119.7	531.4
	PSW	in	313.7	191.6	169.0	119.4	531.7
		out	313.4	191.3	169.0	119.0	531.3

The findings on platinum were overall similar as in the LPW and HPW poisoned samples. Platinum is clearly metallic and its concentration decreases considerably during the treatment. The supporting elements, again, do not show any significant changes.

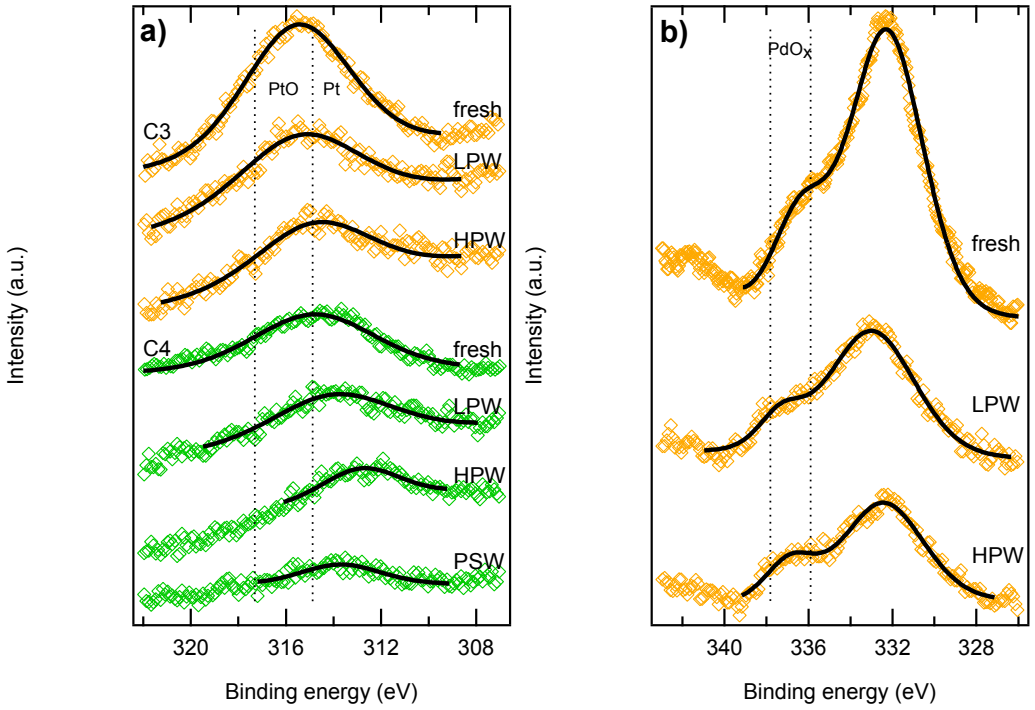

Figure 15: (a) Platinum $4d_{5/2}$ and (b) palladium $3d_{5/2}$ peaks measured from the inlet side of phosphorus poisoned samples C3 and C4. Platinum appears as oxide and metal whereas palladium is oxidic.

5.3 Silica-zirconia supported platinum catalyst for diesel oxidation

5.3.1 Effect of phosphorus poisoning

Similarly to the other DOCs, also the SiO_2-ZrO_2 catalyst (C5) was poisoned with the two phosphorus treatments (LPW and HPW). The equivalent bare washcoat (S5) was only HPW treated. Figure 17 shows the phosphorus 2s lines measured from the inlet sections. As the figure and table 11 show, some deviation is again visible in binding energy values. However, all of them indicate phosphate species [34]. As earlier, based on the atomic percentages in table 12 phosphorus shows preference for inlet adsorption. It was also observed that phosphorus accumulation on the bare washcoat was almost nonexistant. This may suggest an active role for platinum in phosphorus poisoning. On the other hand, it is also possible that the treatment for the particular sample was not successful for some reason.

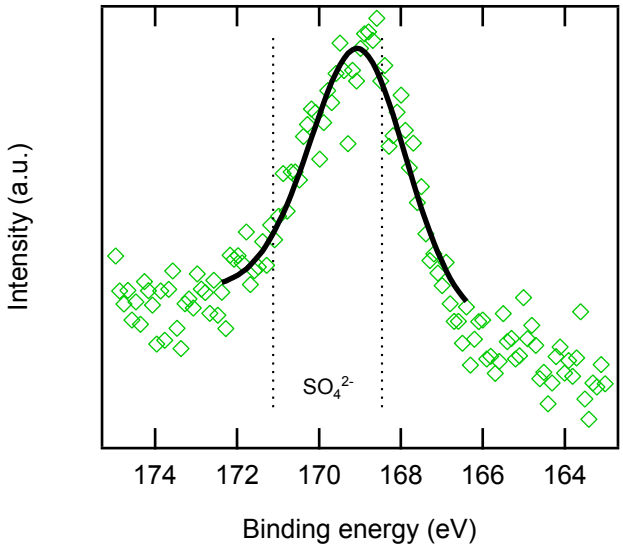

Figure 16: The sulfur 2p peak from the inlet side of PSW poisoned catalyst C4. Sulfur occurs on the surfaces as sulfate.

Table 10: Elemental compositions (in at.%) measured from the fresh and phosphorus-sulfur poisoned DOC samples.

			Pt	P	S	Al	O	Ce	Zr	Si	Ti
Pt	fresh		0.15	-	-	29	66	0.19	0.07	2.1	2.7
catalyst	PSW	in	0.02	4.1	0.67	20	69	0.13	0.06	2.9	2.8
(C4)		out	0.06	1.6	1.3	22	68	0.3	0.16	2.8	3.4

Platinum spectra are shown in figure 18. According to the binding energy values, platinum appears to be metallic in all phosphorus poisoned samples. As usually, some deviation is apparent in the series. However, none of the gained values indicate oxidation of platinum [35]. In all measured samples, the atomic percentage of platinum stayed almost constant. This indicates that phosphorus does not block platinum atoms on the surface very efficiently. Furthermore, this leads to assume that the HPW treatment for S5 did not work out properly, since based on these results it seems unlikely that the bare washcoat were more resistant towards phosphorus poisoning than the actual catalyst.

The washcoat elements did not show any surprising features. Atomic ratio of silicon and zirconium was around 2 : 1 in all samples. Since the washcoat

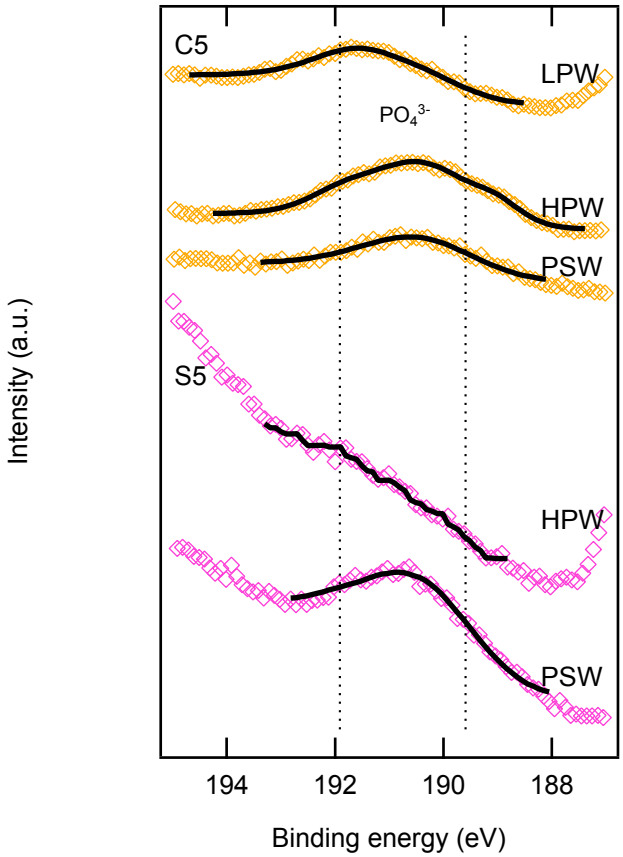

Figure 17: Phosphorus 2s peaks measured from the inlet side of samples C5 and S5 show phosphorus appearing as phosphate.

consists of two oxides, O 1s peaks have two components which was seen as an asymmetry in the peak form. To analyze all the spectra equally, the components were deconvoluted with the data using some restrictions. First, the distance between the two peaks was restricted to be constantly 2.3 eV. The value was chosen in order to have an adequate fit, and using it was justified by tabulated binding energy values of O 1s lines in SiO_2 and ZrO_2 [34]. Second, both peaks within one spectrum were forced to have the same FWHM value. Thus calculated atomic percentages for the different oxygen specimens followed the ratios of Si and Zr, as expected. The same fitting procedure was also used for the O 1s spectra in sections 5.3.2-4.

Table 11: Binding energy values (in eV) of the major XPS lines measured from the fresh and phosphorus poisoned DOC samples.

			Pt $4d_{5/2}$	P 2s	Si 2s	Zr $3d_{5/2}$	O 1s	
Pt catalyst (C5)	fresh		313.1	-	153.4	182.0	532.0	529.7
	LPW	in	314.4	191.4	154.3	183.0	532.2	529.9
		out	313.9	190.4	154.1	182.7	532.4	530.1
	HPW	in	314.1	190.4	153.1	182.3	531.0	528.7
		out	313.2	190.9	153.6	182.2	531.3	529.0
Support (S5)	fresh		-	-	154.0	182.3	532.5	530.2
	HPW	in	-	190.1	154.4	182.5	532.4	530.1
		out	-	190.5	153.0	181.7	531.5	529.2

Table 12: Elemental compositions (in at.%) measured from the fresh and phosphorus poisoned DOC samples.

			Pt	P	Si	Zr	O
Pt catalyst (C5)	fresh		0.05	-	19	9.5	71
	LPW	in	0.04	3.2	15	7.8	74
		out	0.06	0.25	19	9.9	71
	HPW	in	0.05	6.1	13	7.3	74
		out	0.06	5.0	15	6.3	74
Support (S5)	fresh		-	-	19	8.4	72
	HPW	in	-	0.13	20	8.2	72
		out	-	0.08	19	7.3	74

5.3.2 Effect of sulfur poisoning

Catalyst C5 and support S5 were subjected to sulfur poisoning both with S and SW treatments. Tables 13 and 14 show the acquired binding energies and atomic percentages in each sample. Figure 19 shows the S 2p spectra taken in the inlet section of each sample. As with alumina based SW poisoned samples, sulfur was found to have formed sulfate compounds [38]. The same was also observed in the "dry" sulfur poisoned (S treated) samples. Again, some deviation occurs, but not in the extent to imply changes in chemical states. The atomic percentages of sulfur appeared to be really low in all samples. As seen in table 14, sulfur was never found more abundantly than 0.7 at.%. In most cases, much less sulfur was observed. To compare with the earlier studies on alumina based DOCs, the values are one order of magnitude lower. Furthermore, the bare substrate was consistently observed to accumu-

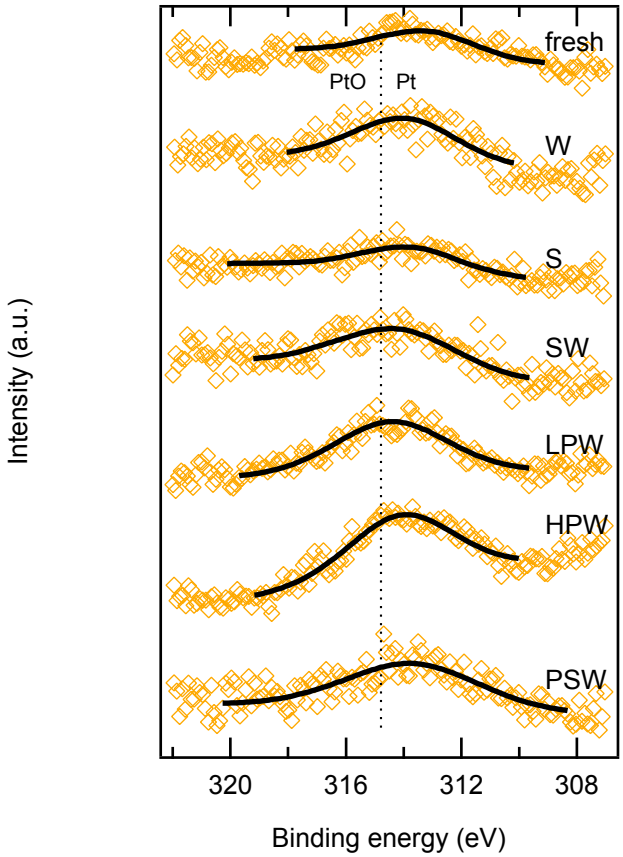

Figure 18: Platinum $4d_{5/2}$ peaks measured from the inlet side of catalyst C5 after various treatments. Platinum is metallic.

late even less sulfur than the catalyst. In addition, the SW poisoned samples showed slightly more sulfur than the S poisoned. Only minor differences were found between inlet and outled ends.

Platinum spectra are again shown in figure 18. The sulfur treatments seem to have had practically no effect on platinum. In all samples, platinum appears to be metallic according to binding energy values [34, 35]. In addition, atomic concentration has not reduced during the treatments. The lack of changes is understandable. Since sulfur seems to accumulate only weakly on the surface, clear changes brought about by it cannot even be expected. None of the elements in the supporting washcoat (Si, Zr, O) showed any changes due to sulfur treatments either.

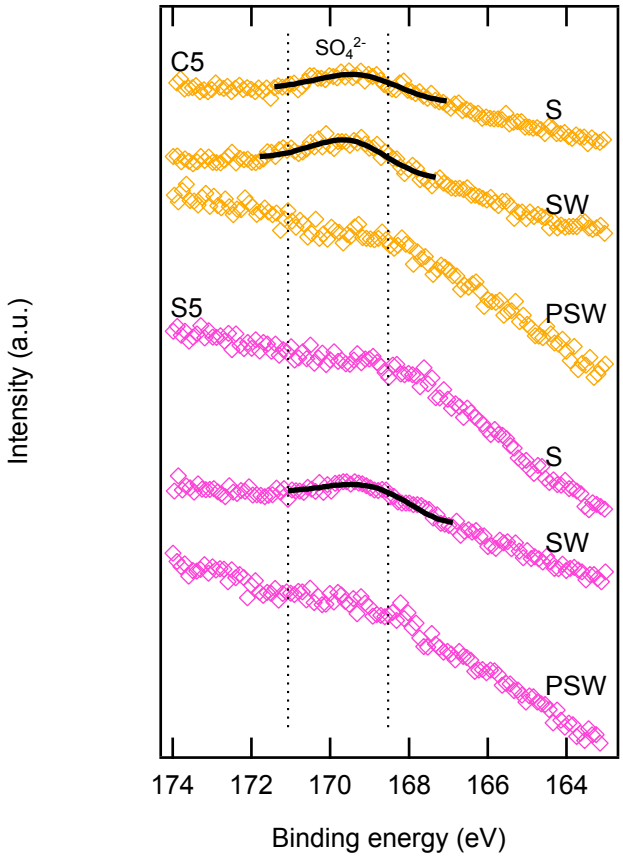

Figure 19: Sulfur 2p peaks measured from the inlet side of samples C5 and S5. There is hardly any sulfur on the surface.

5.3.3 Co-effect of phosphorus and sulfur

C5 and S5 were also PSW treated to see effects of a simultaneous phosphorus and sulfur poisoning. Tables 15 and 16 present the results of these measurements, and figures 17, 19 and 18 show the inlet spectra of P, S and Pt, respectively. Phosphorus adsorption dominates over sulfur, which is not surprising taking the results in previous two sections into account. Phosphorus, like in HPW poisoned samples, gathers preferentially in the inlets. Consequently, sulfur could not be detected at all in the inlets. In the outlet ends however, very little amounts of sulfur were observed. There too, the atomic concentrations were even smaller than in the SW and S treated samples. Atomic concentrations of phosphorus were significantly larger than those of sulfur. In C5, phosphorus concentration was found to be roughly half of the amount after HPW treatment. In S5 the atomic percentage was an order of magni-

Table 13: Binding energy values (in eV) of the major XPS lines measured from the fresh and sulfur poisoned DOC samples.

			Pt $4d_{5/2}$	S 2p	Si 2s	Zr $3d_{5/2}$	O 1s	
Pt catalyst (C5)	fresh		313.1	-	153.4	182.0	532.0	529.7
	S	in	313.6	169.2	153.8	182.7	532.3	530.0
		out	314.5	169.1	153.8	182.7	532.5	530.2
	SW	in	314.1	169.4	154.6	183.1	533.4	531.1
		out	314.3	169.8	153.8	182.6	532.6	530.3
Support (S5)	fresh		-	-	154.0	182.3	532.5	530.2
	S	in	-	-	153.6	182.3	532.3	530.0
		out	-	168.7	153.7	181.9	531.9	529.6
	SW	in	-	168.8	153.8	182.3	532.0	529.7
		out	-	169.8	153.6	182.7	532.4	530.1

tude larger than after HPW treatment and thus comparable to the values seen in C5. This further confirms the assumption than the low P concentrations in S5 reported in section 5.3.1 were due to an unsuccessful treatment. Phosphorus 2s lines again suggest there are phosphate species on the surface [34]. Similarly, sulfur 2p lines, where visible, indicate sulfate compounds [36].

Platinum was again observed to be metallic. As was the case with separate phosphorus and sulfur treatments, the PSW treatment did not seem to change the chemical state or atomic concentration of platinum. All in all, the findings in the PSW poisoned catalyst sample were almost identical to those in LPW and HPW treated ones, whereas presence of sulfur was found to be practically negligible. In section 5.2.2 it was concluded that phosphorus dominated over sulfur in the alumina-supported DOC. Here however, the domination is definitely remarkably stronger.

5.3.4 Effect of hydrothermal aging

Hydrothermal aging (or "water poisoning", W in table 2) was carried out on C5 and S5 to extract the possible effects of water in the poisoning gas mixtures or temperature during the treatments. The treatment was otherwise similar to the SW, LPW and HPW processes, but the gas mixture did not include sulfur dioxide nor did the water vapour include ammonium phosphate. The XPS results of the treated samples are shown in tables 17 and 18. Pt $4d_{5/2}$ line from the inlet side is shown again in figure 18. As it can be seen in the tables, platinum stays metallic, and its atomic concentration

Table 14: Elemental compositions (in at.%) measured from the fresh and sulfur poisoned DOC samples.

			Pt	S	Si	Zr	O
Pt catalyst (C5)	fresh		0.05	-	19	9.5	71
	S	in	0.07	0.33	19	8.3	72
		out	0.09	0.35	18	8.6	73
	SW	in	0.08	0.35	19	7.5	73
		out	0.07	0.68	17	8.4	74
Support (S5)	fresh		-	-	19	8.4	72
	S	in	-	0.00	19	9.4	72
		out	-	0.15	21	6.9	72
	SW	in	-	0.19	19	8.3	72
		out	-	0.18	19	9.3	71

Table 15: Binding energy values (in eV) of the major XPS lines measured from the fresh and phosphorus-sulfur poisoned DOC samples.

			Pt $4d_{5/2}$	P 2s	S 2p	Si 2s	Zr $3d_{5/2}$	O 1s	
C5	fresh		313.1	-	-	153.4	182.0	532.0	529.7
	PSW	in	313.6	190.4	-	153.6	182.1	531.6	529.3
		out	313.9	190.7	168.8	153.8	182.1	532.2	529.9
S5	fresh		-	-	-	154.0	182.3	532.5	530.2
	PSW	in	-	190.3	-	153.7	182.0	531.8	529.5
		out	-	190.2	170.8	153.6	181.9	532.3	530.0

does not show decrease. The elements in the substrate do not show any interesting features either. There are no noteworthy differences between the inlet and outlet sections. Therefore, it can be concluded that the hydrothermal treatment provides no such effects that could be observed with XPS. Water does not seem to cause any chemical changes, and the temperature of 400 °C appears not to be high enough for thermal effects to occur.

Table 16: Elemental compositions (in at.%) measured from the fresh and phosphorus-sulfur poisoned DOC samples.

			Pt	P	S	Si	Zr	O
Pt catalyst (C5)	fresh		0.05	-	-	19	9.5	71
	PSW	in	0.09	3.1	0.00	16	6.7	74
		out	0.06	1.5	0.08	16	7.3	75
Support (S5)	fresh		-	-	-	19	8.4	72
	PSW	in	-	1.5	0.00	17	7.1	74
		out	-	0.35	0.15	19	7.9	73

Table 17: Binding energy values (in eV) of the major XPS lines measured from the fresh and hydrothermally aged DOC samples.

			Pt $4d_{5/2}$	Si 2s	Zr $3d_{5/2}$	O 1s	
Pt catalyst (C5)	fresh		313.1	153.4	182.0	532.0	529.7
	W	in	313.9	153.7	181.9	532.2	529.9
		out	314.8	154.3	181.8	532.6	530.3
Support (S5)	fresh		-	154.0	182.3	532.5	530.2
	W	in	-	153.6	182.0	532.1	529.8
		out	-	154.0	182.3	532.5	530.2

Table 18: Elemental compositions (in at.%) measured from the fresh and hydrothermally aged DOC samples.

			Pt	Si	Zr	O
Pt catalyst (C5)	fresh		0.05	19	9.5	71
	W	in	0.06	20	7.5	72
		out	0.07	19	8.4	72
Support (S5)	fresh		-	19	8.4	72
	W	in	-	19	9.0	72
		out	-	19	9.1	72

5.4 Accuracy and repeatability

In order to evaluate the reliability of the XPS studies, several samples were measured more than once. As an example, the inlet section of the PSW treated catalyst C5 was measured and analyzed six times. The acquired binding energy values and atomic concentrations are shown in tables 19 and 20, respectively.

Table 19: Binding energy values (in eV) of the major XPS lines measured repeatedly from the inlet section of the PSW treated catalyst C5.

Ref.	Pt $4d_{5/2}$	P 2s	S 2p	Si 2s	Zr $3d_{5/2}$	O 1s	
1	313.6	190.4	167.8	153.6	182.1	531.6	529.3
2	313.6	190.5	-	153.3	181.3	531.5	530.3
3	313.9	190.5	168.4	153.5	181.7	531.8	530.0
4	313.6	190.2	168.9	153.1	181.7	531.6	530.1
5	313.2	190.1	167.9	153.3	181.3	531.4	529.9
6	313.4	190.4	167.8	153.3	182.0	531.3	529.4

Table 20: Elemental compositions (in at.%) measured repeatedly from the inlet section of the PSW treated catalyst C5.

Ref.	Pt	P	S	Si	Zr	O
1	0.085	3.05	0.045	16.2	6.6	74.0
2	0.064	2.22	0.000	15.0	6.4	76.3
3	0.059	3.34	0.025	13.8	7.1	75.7
4	0.053	3.13	0.029	14.9	6.5	75.4
5	0.064	3.10	0.013	14.9	6.6	75.3
6	0.047	4.19	0.047	13.1	6.2	76.5

The binding energy variation seen in phosphorus is 0.4 eV. The deviations are small and come mainly from differences in fitting and energy calibration. The interpretation of the results is not altered anyhow, as all the acquired values represent phosphate. Platinum peaks have an energy range of 0.7 eV. However, all the measured values indicate metallic platinum. The washcoat elements feature deviations of same magnitude although their XPS lines are more clearly visible. This suggests the C 1s calibration is the main source for binding energy alterations. It must also be pointed out that in this series, the

two oxygen peaks caused by ZrO_2 and SiO_2 were fitted without the fixed energy difference of 2.3 eV, which may also have caused some further deviations.

As noted in section 5.3.3, sulfur was practically undetected in the PSW treated C5 samples. The values in tables 19 and 20 represent the features in the S 2p region of the spectrum. No peaks were seen and practically the fitting was made to the background. Therefore it is justified to conclude that sulfur could not be found at all. Also the atomic percentages shown in table 20 are one order of magnitude smaller than in those samples where sulfur could actually be seen (table 14).

The atomic percentages of phosphorus are in most cases slightly above 3% but vary from 2.2 to 4.2%. However, the results are clearly in the same order of magnitude, and furthermore, the changes are not as significant as have been seen between different samples. The same can be concluded for platinum. Its atomic concentration was also seen to change almost with a factor of 2, but the alterations are not larger than those seen after different treatments. Furthermore, the washcoat elements exhibited only slight changes in atomic percentages. Since they form larger photoemission peaks, the way the fit is chosen or the background is formed around can have only relatively small effect on the atomic concentration. Oxygen and silicon, the two most abundant elements on the surface have a combined atomic concentration ranging from 89.5 to 91.5%.

The results gained from this sample can be generalized, since all other samples have been measured in the same way. Both the binding energy and the atomic concentration analyses indicate that the measurements are adequately repeatable. If it were necessary, the accuracy of atomic percentages of minor elements could be improved by measurements with increased number of scans.

6 Discussion

6.1 Further analysis with complementary methods

The purpose of these studies was to gain information on how chemical and thermal treatments change the studied catalysts. The results that XPS measurements have provided, i.e. elemental compositions, chemical compounds and changes in these two, are only one facet of the studies. In the course of the work several other methods have been employed in order to fill in the picture from different points of view. For instance, scanning electron microscopy (SEM) and transmission electron microscopy (TEM) have been used for characterizing structural changes in the noble metals, distribution of the catalyst poisons and other topographic properties. Activity tests (mentioned also in section 5.1.2) have been applied to see how the treatments actually affect the ability of a catalyst to convert exhaust gases. Nitrogen adsorption measurements were carried out to characterize specific surface areas, pore sizes and pore volumes in the washcoats according to Brunauer-Emmett-Teller (BET) and Barrett-Joyner-Halenda (BJH) theories. In addition to these, for example diffuse reflectance infrared Fourier transform spectroscopy (DRIFT) and X-ray diffraction (XRD) were used. However, not all methods of measurements were applied to every series of catalysts.

6.1.1 Phosphorus on Pt-Pd/Al_2O_3 natural gas oxidation catalyst

In the XPS measurements of phosphorus poisoned NGO catalysts (C1, C2 and S1, section 5.1.1), phosphorus was found to strongly prefer inlets. HPW treatment produced higher accumulation of phosphorus than LPW, although the difference was not immense. Phosphorus was found to be on the surface as a part of a phosphate compound. Platinum and palladium were found oxidized, and phosphorus treatments reduced their atomic concentrations to some extent. The washcoat without noble metals showed overall similar behaviour although larger amounts of phosphorus were found on the surface.

Also TEM and SEM studies indicate that phosphorus resides in larger quantities in the inlet ends. Moreover, SEM has shown that in C1 phosphorus is found in the topmost parts of the sample more profoundly than in areas below. This marks a significant difference to S1 in which the phosphorus distribution was independent of depth. However, the microscopy studies have also shown that the catalysts bear no uniform structure, and phosphorus concentration varies locally. In addition, SEM studies show no morphological changes in a fresh C1 catalyst, in neither LPW nor HPW treated samples.

Activity measurements showed that phosphorus had significant effect on methane (CH_4) oxidation capability. LPW treatment decreased the conversion rate 14 and HPW almost 40 percent. Light-off temperature for methane conversion (50% efficiency) was observed to rise ca. 30 °C for LPW and ca. 100 °C for HPW treated samples. Similar values were found for CO oxidation (90% efficiency). [39]

The BET and BJH studies have shown that the LPW treatment reduces the specific surface area of C1 by roughly 20% and HPW by 30%. For S1 the respective values are nearly 30% and 40%. For comparison, a W treated C1 sample has been studied with the method as well, and no changes were observed. Since there was no hydrothermal effect, it can be concluded that the treatment temperature is too low for thermal sintering to occur. This further indicates that structural changes are all caused by phosphorus adsorption. In addition, the result goes well along with the microscopy studies where no extensive morphological changes were observed. [39]

XRD studies on C1 agree with XPS on phosphorus appearing as phosphate. Furthermore, they suggest that phosphorus is $AlPO_4$, which is reasonable, since aluminum is the most abundant metal on the surface. XRD studies also suggest partial reduction of platinum which was not seen in XPS. [39]

6.1.2 Sulfur on thermally aged Pt-Pd/Al_2O_3 natural gas oxidation catalyst

The combined SW and TA treatments for catalyst C1 were studied in section 5.1.2. Sulfur was found as sulfate, and whether thermal aging was carried out prior to sulfur poisoning did not have significant effect on the sulfur line. When TA treatment was done after SW treatment, sulfur was hardly found on the surface at all, as it is most likely desorbed. Also performing activity measurement was found to diminish sulfur concentration. Palladium was found as oxide, except after activity measurements where it was clearly reduced as metallic. Platinum was oxide too in the SW treated sample, but after thermal treatment it could not be found on the surface anymore.

SEM studies show that sulfur is uniformly located throughout the catalyst, from inlet to outlet and from the surface down to monolith interface. Otherwise, there are no remarkable morphological alterations to a fresh catalyst. With TEM it is seen that in a fresh catalyst platinum and palladium form clusters with diameter typically less than 5 nm. Sulfur poisoning increases

the size of the clusters only slightly. In all TA treated samples, effects of sintering have been observed. Noble metal particle sizes are significantly grown, as the diameter can be even 60 nm. The large particles consist of metallic Pt-Pd core and a PdO shell. This also provides an explanation why platinum was not seen with XPS in the thermally aged samples. Due to the surface sensitivity of the method only the PdO shells are observed but platinum and metallic palladium underneath are left undetected. Sulfur was not seen at all in the SW + TA treated sample with SEM or TEM. BET and BJH analyses follow the same trends. Surface specific area decreases ca. 5% as a consequence of SW treatments. Much more prominent changes take place during TA treatments. 40% decrease in specific surface area and correspondingly 40% increase in pore size have been found. [40]

Activity tests show that despite the more significant structural changes occurring during TA treatment, sulfur poisoning has an equally significant effect on conversion activity. Mechanisms behind are naturally different. Thermal aging causes particle size growth thus decreasing the number of active sites whereas sulfur blocks them. Both have been observed to cause about 100 °C increase in needed temperature for catalytic reactions to take place yet neither actually decreases CH_4 conversion rate more 5%. TA + SW treatment worsen the activity much more, decreasing the methane conversion rate by 20%. Beside XPS, no other measurements were done to a sample having gone through an activity test. However, the palladium reduction observed can be explained by methane oxidation [41]. [40]

6.1.3 Phosphorus and sulfur on Pt-Pd/Al_2O_3 and Pt/Al_2O_3 diesel oxidation catalysts

Effects of phosphorus poisoning of alumina-based DOC samples C3, C4 and S3/4 were discussed in section 5.2.1. Again, phosphorus was found as phosphate and had a preference for inlet adsorption. Palladium was oxidized, and its concentration was seen clearly to decrease in phosphorus poisoned samples. Platinum too was oxidized in the presence of palladium in C3, but in C4 where there was no palladium, platinum was metallic. The atomic concentration of platinum decreased significantly more in C4 than in C3. In a PSW poisoned sample (section 5.2.2) phosphorus was seen to behave similarly as in HPW or LPW treated samples. Sulfur was detected as sulfate, and was seen to gather more in the outlet section, where there was less phosphorus.

Microscopy studies have shown that the morphology of active metal particles in C3 differs remarkably from that of C4. In the fresh C3 catalyst

palladium and platinum form joint particles smaller than 5 nm in diameter. The LPW treatment slightly increases these particles but in HPW treated samples the increase is more notable. In a fresh C4 catalyst, larger (5-10 nm) irregularly shaped platinum crystals have been found instead. After both LPW and HPW treatments, more spherical Pt crystals have been detected. In both Pt and Pt-Pd catalyst, the noble metal particles have been observed to reside in areas with alumina, titania, ceria and zirconia, but not in the areas with silica. In agreement with XPS results, a preference for phosphorus adsorption on the inlet sites has also been found with SEM studies. However, the distribution of phosphorus varies a lot depending on the local support composition. In silica-rich areas, the phosphorus content is lower than elsewhere. This implies phosphorus forming aluminum phosphate ($AlPO_4$), a result which is also suggested by XRD measurements. The HPW treatment results in a larger phosphorus concentration in both catalysts. The strong local variation may explain why the opposite was observed in XPS studies of C3. Furthermore, the overall morphological changes are more clearly visible after the HPW treatment. The SEM and TEM studies of a PSW treated catalyst (C4) are in a strong agreement with XPS results. Phosphorus clearly prefers the inlet section and could not be detected at all in the outlet. On the other hand, more sulfur has been seen in the outlet than in the inlet. Moreover, phosphorus prefers to be on the surface. At 40 micrometres deep, sulfur has been seen to actually dominate in the inlet section as well. [42]

BET and BJH studies indicate significant changes in specific surface areas and pore volumes due to the phosphorus treatments. Both the surface areas and the pore volumes decrease by roughly 30% in C3 and 40% in C4 during the HPW treatment. In the bare support (S3/4) the decrease was observed to be the largest, ca. 50%. A W treated sample has also been studied, but no changes have been detected suggesting that phosphorus is behind all the structural changes, not temperature. [43]

The influence of phosphorus on CO, C_3H_6 and NO oxidation activity has been studied. The LPW treatment for both C3 and C4 only increases the light-off temperature for propene conversion, but otherwise it has almost no effect. In HPW poisoned samples, the catalytic ability is much more reduced, as the maximum conversion rates drop by 10-20 percent for carbon monoxide and propene. The decline has been found stronger in the Pt-Pd catalyst (C3). As for NO, the oxidation reaction is almost totally inhibited. Therefore, also the activity test results suggest that there ought to be more phosphorus in a HPW treated C3 than in LPW treated one. [43]

6.1.4 Phosphorus and sulfur on Pt/SiO_2-ZrO_2 diesel oxidation catalyst

The Pt/SiO_2-ZrO_2 catalyst C5 and the washcoat S5 were subjected to a large series of different measurements. Hydrothermal treatment did not have any effect on the XPS results. Sulfur appeared not to stick efficiently on the catalyst or support surface. The acquired atomic concentrations were consistently less than 1%, which is much smaller coverage than what has been found in previous studies on alumina-based DOC surfaces [37]. Sulfur, where visible, was interpreted as a part of a sulfate compound. Phosphorus treatments had a more profound effect, as atomic concentrations up to 6% were observed. Phosphorus, like in all other measured catalysts, followed a trend of selective adsorption on the inlet surface. Likewise, it was detected to be phosphate, as before. A PSW poisoned sample was similar to phosphorus-only poisoned samples, albeit there was a trace of sulfur detected in the outlet end and the amount of phosphorus was found smaller.

Microscopy studies of C5 and S5 are in agreement with results gained with XPS. Only very little amounts of sulfur have been found throughout the sample. The distribution of sulfur is uniform in all three dimensions. Phosphorus poisoning in a HPW treated sample has been found to be much more efficient than sulfur poisoning. A slightly higher concentrations in the inlet side have been found, but within the top-bottom axis the distribution is uniform. The behaviour of phosphorus and sulfur is similar in both the catalyst and the washcoat without noble metals. The phosphorus content has been detected lower than it was in an alumina-based platinum DOC (C4). This is understandable, since in C4 the silica-rich area lacked phosphorus. This suggests that silica may be somewhat resistant against phosphorus poisoning too. For sulfur, this clearly seems to be the case, as some earlier reports also state [21]. The PSW treated sample has appeared to be almost identical to HPW treated one in SEM and TEM studies. The accumulation and appearance of phosphorus is similar, and sulfur cannot be detected at all.

BET and BJH studies also indicate that the effect of sulfur is negligible. The S treatment does not cause changes in the surface area or pore volume values at all. In SW treatment the specific surface area is reduced by 10%. However, the W treatment has given a 7% reduction implying the change is mostly if not at all due to water, not sulfur. The changes are similar in the support material as well. For comparison, after the HPW and PSW treatments decreases of ca. $40-70\%$ and $20-50\%$ are seen in specific surface area and pore volume, respectively. No clear differences between C5 and S5 were

found. This implies that phosphorus reacts with the substrate regardless the presence of platinum. [44]

Again, CO, C_3H_6 and NO conversion activity has been tested. Sulfur or water has no effect to conversion of propene or carbon monoxide. An S treated sample behaves like a fresh one in NO conversion, but W and SW treatments decrease the conversion rate by 10%, coinciding with the specific surface area reduction rate. This again suggests that water may effect the catalyst more than sulfur does. HPW and PSW treatments increase light-off temperatures of CO and C_3H_6 oxidation and decrease NO conversion rate by ca. 20%. The deactivation is clearly more profound than in a sulfur treated catalysts, but probably not as remarkably as the structural differences might imply. The deactivation is somewhat stronger after the HPW treatment, which together with the XPS results implies that sulfur actually inhibits phosphorus poisoning. [44]

6.2 The role of the XPS analysis

As the preceding section shows, the XPS measurements were only one part in a long line of experiments. Moreover, the information that can be acquired from XPS is of course quite limited in the end. Therefore, it is clear that with XPS alone it is not possible to carry out a catalyst poisoning study, and as noticed in some cases, structural studies were needed to even interpret the XPS results. Nevertheless, as a part of a versatile catalyst study XPS is a very profitable technique. Its benefit is the large library of readily available data for analysis. However, especially when elemental concentrations are small, it may be difficult to have the surface completely characterized. For example in this work, sulfur and phosphorus were found to be as sulfate and phosphate, respectively, but the complete molecules could not be distinguished. Similarly, the oxygen in the sulfate and phosphate molecules was never observed because oxygen in the washcoat oxides dominated the O 1s region.

As discussed in section 5.4, the XPS measurements have an adequate repeatability. It needs to be pointed out that the sample surfaces are not homogeneous as the structural studies have shown. This can possibly cause deviations in the XPS results. However, since the structural features are tens of nanometres in size, and the used X-ray spot size wass at least 600 micrometres, some averaging has taken place by itself in the XPS results.

Some further analysis with XPS would be potential. By sputtering the surface, some chemical changes between surfaces and inner structures could

possibly be seen. However, since the measurements need to be done with scraped catalyst, depth profiling from the surface to the monolith would not be conceivable anyway. Another approach, yet beyond the capability of the system used in this work, could be chemical mapping. The distribution of different elements, mainly poisons and noble metals could be characterized with lateral X-ray scans. These studies could further confirm the results found in microscopy studies.

6.3 Conclusions

This work presents a collection of XPS results of laboratory-aged DOC and NGO catalyst samples. The main emphasis is on phosphorus poisoning, but effects of sulfur poisoning and thermal treatment on some catalysts have also been studied. The primary tasks have been to determine how strongly the poison particles accumulate on the surface, what compounds they form and how they influence the catalytic noble metal particles on the sample surface. XPS gives answers to these questions in terms of binding energy shifts induced by chemical changes, and relative elemental concentrations.

Behaviour of phosphorus was qualitatively similar in all studied catalysts. Larger concentrations were generally seen in inlet sections and phosphorus always appeared as a part of a phosphate compound (PO_4^{3-}). Phosphorus accumulation was stronger on alumina than on silica-zirconia washcoats. The presence of phosphorus was found to diminish atomic concentrations of noble metals platinum and palladium, but their chemical state was not seen to unambiguously change due to phosphorus treatment. The spectra of carrier elements within the catalyst washcoats did not show notable differences between fresh and phosphorus poisoned catalyst samples. Phosphate formation with washcoat elements is probable but cannot be detected in XPS for certain.

In sulfur-phosphorus poisoned catalyst samples the behaviour of phosphorus was virtually identical to what had been found in phosphorus-only poisoned catalysts. In earlier studies sulfur was seen to be uniformly distributed, but in the presence of phosphorus it was mainly found in the outlet section where phosphorus is not as prominent. This suggests that sulfur and phosphorus compete for the same adsorption sites and phosphorus is more dominant. On silica-zirconia-supported catalysts sulfur adsorption was seen to be almost entirely prevented. In all samples where sulfur was detected, it appeared as a part of a sulfate compound (SO_4^{2-}).

XPS measurements were accompanied by many other studies carried out elsewhere, concentrating on catalyst structures and activity, for instance. The XPS results acquired on the phosphorus and sulfur poisoned samples were well in line with those. Furthermore, the results were following the lines that have been reported before in studies of comparable catalysts.

XPS results of a thermally aged Pt-Pd catalyst showed disappearance of platinum peaks. This was explained by microscopy studies that indicated sintering of the catalyst particle. Furthermore, thermal treatment was shown to decrease sulfur content on the sample surface, suggesting sulfur desorption and possibly partial regeneration of catalytic activity.

References

[1] Regulation (EC) No 715/2007 of the European Parliament and of the Council on type approval of motor vehicles with respect to emissions from light passenger and commercial vehicles (Euro 5 and Euro 6) and on access to vehicle repair and maintenance information, 2007

[2] R. M. Heck, R. J. Farrauto, Appl. Catal. A 221 (2001) 443-457

[3] D. A. Lashof, D. R. Ahuja, Nature 344 (1990) 529-531

[4] Trafi – Finnish Transport Safety Agency, URL: http://www.trafi.fi/tietopalvelut/analyysitoiminta/indikaattorit/ymparistoindikaattorit/liikenteen_paastot_ilmaan, retrieved 18.5.2015

[5] D. G. Streets, S. T. Waldhoff, Atmos. Environ. 34 (2000) 363-374

[6] T. J. Wallington, E. W. Kaiser, J. T. Farrell, Chem. Soc. Rev. 35 (2006) 335-347

[7] R. M. Heck, R. J. Automotive Eng. Feb. (1996) 93-96

[8] M. Honkanen, M. Kärkkäinen, V. Viitanen, O. Heikkinen, H. Jiang, K. Kallinen, M. Huuhtanen, J. Lahtinen, R. Keiski, M. Vippola, T. Lepistö, XIth European Congress on Catalysis (2013) poster presentation

[9] M. Kärkkäinen, T. Kolli, M. Honkanen, O. Heikkinen, K. Kallinen, M. Vippola, T. Lepistö, J. Lahtinen, R. L. Keiski, 16th Nordic Symposium on Catalysis (2014) poster presentation

[10] H. S. Gandhi, G. W. Graham, R. W. McCabe, J. Catal. 216 (2003) 433-442

[11] R. J. Farrauto, R. M. Heck, Catal. Today 51 (1999) 351-360

[12] S. M. Park, H.-G. Jang, E. S. Kim, H.-S. Han, G. Seo, Appl. Catal. A 427-428 (2012) 155-164

[13] C. T. Goralski Jr., W. F. Schneider, Appl. Catal. B 37 (2002) 263-277

[14] N. Nejar, M. Makkee, M. J. Illán-Gómez, Appl. Catal. B 75 (2007) 11-16

[15] A. Russell, W. S. Epling, Catal. Rev.: Sci. and Eng. 53:4 (2011) 337-423

[16] D. L. Mowery, M. S. Graboski, T. R. Ohno, R. L. McCormick, Appl. Catal. B 21 (1999) 157-169

[17] J. K. Lampert, M. Shahjahan Kazi, R. J. Farrauto, Appl. Cat. B 14 (1997) 211-223

[18] P. Gélin, M. Primet, Appl. Catal. B 39 (2002) 1-37

[19] P. Forzatti, L. Lietti, Catal. Today 52 (1999) 165-181

[20] C. H. Bartholomew, Appl. Catal. A 212 (2001) 17-60

[21] A. K. Neyestanaki, F. Klingstedt, T. Salmi, D. Yu. Murzin, Fuel 83 (2004) 395-408

[22] M. J. Rokosz, A. E. Chen, C. K. Lowe-Ma, A. V. Kucherov, D. Benson, M. C. Paputa Peck, R. W. McCabe, Appl. Catal. B 33 (2001) 205-215

[23] R. Beckmann, W. Engeler, E. Mueller, B. Engler, J. Leyrer, E. S. Lox, K. Ostgathe, SAE Technical Paper 922330 (1992)

[24] D. Briggs, J. T. Grant, Surface Analysis by Auger and X-Ray Photoelectron Spectroscopy (2003) IM Publications and SurfaceSpectra Ltd., Trowbridge, UK

[25] A. M. Venezia, Catal. Today 77 (2003) 359-370

[26] F. P. J. M. Kerkhof, J. A. Moulijn, J. Phys. Chem 83 (1979) 1612-1619

[27] J. H. Scofield, Lawrence Livermore Laboratory Report UCRL-51326 (1973)

[28] M. P. Seah, W. A. Dench, Surf. Interface Anal. 1 (1979) 2-11

[29] D. A. Shirley, Phys. Rev. B 5 (1972) 4709

[30] M. Aronniemi, J. Sainio, J. Lahtinen, Surf. Sci 578 (2005) 108-123

[31] M. Aronniemi, Development of XPS data analysis and its application to gas sensor and catalyst surface studies, Doctoral dissertation (2007) Helsinki University of Technology

[32] J. C. Fuggle, S. F. Alvarado, Phys. Rev. A 22 (1980) 1615

[33] T. L. Barr, S. Seal, J. Vac. Sci. Technol., A 13 (1995) 1239

[34] A. V. Naumkin, A. Kraut-Vass, S. W. Gaarenstroom, C. J. Powell, NIST X-ray Photoelectron Spectroscopy Database, National Institute of Standards and Technology (2012) URL: srdata.nist.gov/xps

[35] J. Z. Shyu, K. Otto, Appl. Surf. Sci. 32 (1988) 246-252

[36] J. F. Moulder, W. F. Stickle, P. E. Sobol, K. D. Bomben, Handbook of X-ray Photoelectron Spectroscopy (1992) Perkin-Elmer Corporation, Eden Prairie, Minnesota, USA

[37] V. Viitanen, Characterization of poisoned exhaust gas catalysts using X-ray photoelectron spectroscopy, Licentiate thesis (2013) Aalto University

[38] M. Kärkkäinen, M. Honkanen, V. Viitanen, T. Kolli, A. Valtanen, M. Huuhtanen, K. Kallinen, M. Vippola, T. Lepistö, J. Lahtinen, R. L. Keiski, Top. Catal. 56 (2013) 672-678

[39] M. Kärkkäinen, T. Kolli, M. Honkanen, O. Heikkinen, A. Väliheikki, M. Huuhtanen, K. Kallinen, J. Lahtinen, M. Vippola, R. L. Keiski, (2015) in preparation

[40] M. Honkanen, M. Kärkkäinen, T. Kolli, O. Heikkinen, V. Viitanen, L. Zeng, H. Jiang, K. Kallinen, M. Huuhtanen, R. L. Keiski, J. Lahtinen, E. Olsson, M. Vippola, Appl. Catal. B (2015), submitted

[41] P. Castellazzi, G. Groppi, P. Forzatti, Appl. Catal. B 95 (2010) 303-311

[42] M. Honkanen, M. Kärkkäinen, O. Heikkinen, K. Kallinen, T. Kolli, M. Huuhtanen, J. Lahtinen, R. L. Keiski, T. Lepistö, M. Vippola, Top. Catal. (2015) in press, DOI 10.1007/s11244-015-0465-y

[43] M. Kärkkäinen, T. Kolli, M. Honkanen, O. Heikkinen, M. Huuhtanen, K. Kallinen, T. Lepistö, J. Lahtinen, M. Vippola, R. L. Keiski, Top. Catal. (2015) in press, DOI 10.1007/s11244-015-0464-z

[44] A. Väliheikki, T. Kolli, M. Kärkkäinen, M. Honkanen, O. Heikkinen, K. Kallinen, M. Huuhtanen, M. Vippola, J. Lahtinen, R. L. Keiski, (2015) in preparation